UNIVERSITI TEKNOLOGI MARA

EFFECTS OF VELOCITY SLIP ON UNSTEADY MAXWELL FLUID FLOW OVER A STRETCHING SURFACE

JAMALIAH BINTI ABD KARIM

BSc

July 2025

UNIVERSITI TEKNOLOGI MARA

EFFECTS OF VELOCITY SLIP ON UNSTEADY MAXWELL FLUID FLOW OVER A STRECHING SURFACE

JAMALIAH BINTI ABD KARIM

Report submitted in fulfilment
of the requirements for the degree of
Bachelor of Science in Mathematical Modelling and Analytics
Honours

Faculty of Computer and Mathematical Sciences

July 2025

APPROVED BY:

……..

ZANARIAH BINTI MOHD YUSOF

Supervisor

Faculty of Computer and Mathematical Sciences

Universiti Teknologi MARA

Terengganu Branch

Kuala Terengganu Campus

DECLARATION BY THE CANDIDATE

I certify that this report and the project to which it refers is the product of my own work and that any idea or quotation from the work of the other people, published or otherwise are fully acknowledged in accordance with standard referring practices of the discipline.

……..

[JAMALIAH BINTI ABD KARIM]

[2022453136]

Faculty of Computer and Mathematical Sciences

Universiti Teknologi MARA

Terengganu Branch

Kuala Terengganu Campus

ABSTRACT

This study investigates the effects of velocity slip on unsteady magnetohydrodynamic (MHD) flow of a Maxwell fluid over a stretching surface, considering thermal radiation, magnetic fields, porosity, and heat generation/absorption. The governing partial differential equations are transformed into nonlinear ordinary differential equations using similarity variables and solved numerically using the Runge-Kutta-Fehlberg (RKF45). Results demonstrate that velocity slip reduces near-surface fluid velocity while slightly increasing heat transfer, magnetic fields enhance flow resistance without significantly affecting thermal profiles, and porosity increases drag while maintaining thermal performance. Additionally, unsteadiness improves heat transfer through enhanced fluid mixing, and higher Prandtl numbers thin the thermal boundary layer for better heat dissipation. The findings are of immense value in the optimization of industrial processes involving viscoelastic fluids, such as polymer processing and thermal management systems, as well as uncover the influence of slip conditions in micro/nanofluidic systems.

ACKNOWLEDGEMENT

It is my priority to thank Allah the Almighty who gave me the force, knowledge, and endurance to conduct this research. In His infinite mercy and guidance this journey would have been impossible.

I feel obliged to thank my supervisor, Madam Zanariah binti Mohd Yusof so much. Her guidance that I would not replace with any amount of money, her infinite patience, and her constructive comments have become the pillar of my research experience. Her field experience and frequent motivation have been significant to my education and, subsequently, career growth. To this extent I am so honored to have been given an opportunity to learn with her.

My heartfelt thanks go to my beloved family for their unconditional love, endless support, and sacrifices. Their prayers and encouragement have been my pillars of strength, motivating me to overcome challenges and stay focused on my goals.

I would also like to extend my sincere appreciation to my friends and colleagues for their companionship, moral support, and stimulating discussion, which have enriched my research experience. A special mention goes to my mates for their collaboration, making this journey both rewarding and memorable.

Lastly, I am deeply thankful to Universiti Teknologi MARA for providing the necessary resources, facilities, and a conducting academic environment that enabled me to complete this thesis successfully.

TABLE OF CONTENTS

		Page
DECLARATION BY THE CANDIDATE		**iii**
ABSTRACT		**iv**
ACKNOWLEDGEMENT		**v**
TABLE OF CONTENTS		**vi**
LIST OF TABLES		**viii**
LIST OF FIGURES		**ix**
LIST OF SYMBOLS		**x**
LIST OF NOMENCLATURE		**xi**
CHAPTER 1 INTRODUCTION		**13**
1.1	Research Background	13
1.2	Problem Statement	14
1.3	Research Objectives	14
1.4	Significance of Study	15
1.5	Scope of the Project	15
1.6	Definition of Terms and Concept	16
CHAPTER 2 LITERATURE REVIEW		**17**
2.1	Introduction	17
2.2	Literature Review	17
CHAPTER 3 RESEARCH METHODOLOGY		**21**
3.1	Introduction	21
3.1.1	Step 1: Topic Selection	22
3.1.2	Step 2: Understanding the Governing Equation and Boundary Layer	22
3.1.3	Step 3: Incorporating Velocity Slip Condition	24
3.1.4	Step 4: Transforming the Governing Partial Differential Equation into Ordinary Differential Equations	25

3.1.5 Step 5: Numerical Method 26
3.1.6 Step 6: Plotting the Graph 26
3.1.7 Step 7: Analyse the result 26

CHAPTER 4 IMPLEMENTATION 27
4.1 Introduction 27
4.2 Transformation of Partial Differential Equation into Ordinary Differential Equation 27
4.2.1 Continuity equation 34
4.2.2 Momentum equation 35
4.2.3 Energy equation 37
4.2.4 Boundary conditions 39
4.3 Conclusion 44

CHAPTER 5 RESULT AND DISCUSSION 45
5.1 Introduction 45
5.2 Result and Discussion 45
5.3 Result of Skin Friction Coefficient $f''(0)$, Heat transfer Rate $-\theta'(0)$, Velocity Profile and Temperature Profile 46
5.3.1 Velocity slip parameter, λ 46
5.3.2 Various unsteadiness parameter, A 48
5.3.3 Various porosity parameter, K_1 50
5.3.4 Various magnetic parameter, M 52
5.3.5 Various Prandtl number, Pr 54
5.4 Conclusion 55

CHAPTER 6 CONCLUSION AND RECOMMENDATION 56
6.1 Introduction 56
6.2 Conclusion 56
6.3 Recommendation 57

REFERENCES 58
APPENDICES 60

LIST OF TABLES

Tables	Title	Page
Table 1.1	Definition of terms and concept	16
Table 5.1	Comparison of skin friction coefficient $-f''(0)$ with previous study.	45
Table 5.2	$-f''(0)$ and $-\theta'(0)$ when β=0.1, K_1=0.5, Pr=0.7, Ec=0.2, Q=-5.0, S=0.1, M=1.0 and A=0.1 for λ various values.	47
Table 5.3	$-f''(0)$ and $-\theta'(0)$ when β=0.1, K_1=0.5, Pr=0.7, Ec=0.2, Q=-5.0, S=0.1, M=1.0 and λ=0.5 for A various values.	49
Table 5.4	$-f''(0)$ and $-\theta'(0)$ when β=0.1, A=0.1, Pr=0.7, Ec=0.2, Q=-5.0, S=0.1, M=1.0 and λ=0.5 *for* K_1 various values.	51
Table 5.5	$-f''(0)$ and $-\theta'(0)$ when β=0.1, A=0.1, Pr=0.7, Ec=0.2, Q=-5.0, S=0.1, K_1=0.5 and λ=0.5 for M various values.	53
Table 5.6	$-f''(0)$ and $-\theta'(0)$ when β=0.1, A=0.1, M=1.0, Ec=0.2, Q=-5.0, S=0.1, K_1=0.5 and λ=0.5 *for* Pr various values.	55

LIST OF FIGURES

Figures	Title	Page
Figure 3.1	Research flow	21
Figure 3.2	Physical model of fluid flow through stretching surface (Sonam & Yadav, 2024).	23
Figure 5.1	Velocity profile for multiple values of λ	46
Figure 5.2	Temperature profile for multiple values of λ	46
Figure 5.3	Velocity profile for multiple values of A	48
Figure 5.4	Temperature profile for multiple values of A	48
Figure 5.5	Velocity profile for multiple values of K_1	50
Figure 5.6	Temperature profile for multiple values of K_1	50
Figure 5.7	Velocity profile for multiple values of M	52
Figure 5.8	Temperature profile for multiple values of M	52
Figure 5.9	Velocity profile for multiple values of Pr	54
Figure 5.10	Temperature profile for multiple values of Pr	54

LIST OF SYMBOLS

Symbols

η	Similarity variable
υ	kinematic viscosity (m^2 /s)
μ	dynamic viscosity (Ns /m^2)
ρ	fluid density (kg /m^3)
β	Maxwell parameter
λ	velocity slip
α	constant
θ	dimensionless temperature
σ	electric conductivity of the fluid (1 /Ωm)

LIST OF NOMENCLATURE

Nomenclatures

U_W	stretching velocity of the surface (m /s)
Q_0, B_0	constants
c_p	specific heat coefficient
Pr	Prandtl number
C_{f_x}	local skin-friction coefficient
Q^*	heat generation/absorption parameter
Ec	Eckert number
K_1	Porosity parameter
M	magnetic parameter
N	radiation parameter
Nu_x	Nusselt number
A	unsteadiness parameter
S	suction/blowing parameter
k^*	mean absorption coefficient
κ	thermal diffusivity (m^2 /s)
Re_x	Reynolds number
q_r	radiative heat flux
k	thermal conductivity (W /m k)
Q(t)	heat generation/absorption coefficient

T_W	wall temperature (K)
u, v	velocity units (m / s)

CHAPTER 1
INTRODUCTION

1.1 Research Background

The Maxwell fluid is a kind of non-Newtonian fluid that exhibits both viscous and elastic properties. This distinguishes it from ordinary fluids, such as water, which merely exhibit viscosity. Fluid flows across a stretching surface in numerous real-world scenarios, including polymer manufacturing. Heat transport and fluid motion are impacted by these stretched surfaces.

And we find this, that fluid is considered, most commonly in traditional fluid flow, to stick to the surface and not to slip. The claimed assumption is not met in modern technology, in devices with the operation at micro/nano-level. The phenomenon of the fluid moving in contact with the boundary is called velocity slip. The knowledge of this phenomenon is crucial in order to achieve efficient systems, since it strongly affects the flow rate, and the heat exchange close to the surface.

Thermal radiation and magnetic fields are important in the behaviour of fluids, particularly those of heat related, electricity related, or extreme temperature related situations. An example of these porous surfaces is the filters and foams, which can cause substantial effects on fluid flow and heat transfer. The present work is mainly aimed at the influence of the velocity slip on unsteady flow of Maxwell fluids when passing over a stretching surface. The paper takes into consideration the effects of the heat radiation, magnetic fields, and the porous media. The challenge is to have a clarification as to how these factors affect each other and alter the flow characteristics of the fluid and its heat transfer properties.

1.2 Problem Statement

Maxwell fluids are special in that they exhibit both liquid-like and elastic behaviour, and their flow is thus more complicated than usual fluids. Their flow can be influenced by elements such as varying flow conditions with time (unsteadiness), magnetic fields, and heat transfer. One of the significant characteristics that are often overlooked is velocity slip, where fluid partially slips along the surface but not fully adheres, and it becomes crucial in applications like microfluidics, polymer processing, and coated surfaces. Although several studies have performed research on the effects of magnetic fields and heat on Maxwell fluids, the combined effect of velocity slip, unsteady flow, and stretching surfaces has not been investigated extensively yet. Including velocity slip is crucial as it affects greatly boundary layer behaviour, shear stress, and heat transfer rates in engineering processes. In this paper, an attempt is made to numerically investigate the effect of velocity slip on flow and heat transfer of unsteady Maxwell fluids over a stretching surface under the effects of magnetic fields, thermal radiation, porous medium, and internal heat generation. The findings will enhance our understanding of these effects and support better design and control in various industrial and engineering processes.

i. How can similarity variables be used to convert the governing PDEs of unsteady Maxwell fluid flow over a stretching surface into a system of ODEs?

ii. How can the Runge-Kutta-Fehlberg (RKF45) method be effectively implemented to solve the ordinary differential equations?

iii. How do velocity slip, magnetic field, and thermal parameters collectively influence the velocity and temperature profiles in the Maxwell fluid flow?

1.3 Research Objectives

In accordance to the problem statement, the main objectives are

a) to transform the governing partial differential equations into ordinary differential equations using similarity variables.

b) to solve the ordinary differential equation numerically using the Runge-Kutta-Fehlberg (RKF45) method.

c) to analyse how velocity slip, magnetic field strength, porosity, Eckert number, Prandtl number, suction/blowing, and internal heat generation influence the velocity and temperature profiles of the fluid flow.

1.4 Significance of Study

This study provides a deeper understanding of unsteady Maxwell fluid flow with velocity slip over a stretching surface, a topic with limited coverage in existing literature. By incorporating the effects of magnetic fields, thermal radiation, porosity, and heat generation, the research offers a more realistic model applicable to modern engineering systems. The findings are particularly relevant to industries involving microfluidics, polymer processing, and thermal management, where surface slip and non-Newtonian behaviour significantly influence performance. The numerical analysis enhances the theoretical foundation for modelling such flows and supports the development of more efficient thermal and fluid systems.

1.5 Scope of the Project

This project investigates the unsteady flow and heat transfer of an incompressible Maxwell fluid over a stretching surface with velocity slip. The effects of a magnetic field, thermal radiation, porous medium, heat generation or absorption, and viscous dissipation are included. The governing equations are transformed using similarity variables and solved numerically using the Runge-Kutta-Fehlberg (RKF45). The study focuses on how key parameters such as slip, magnetic field strength, porosity, radiation, and unsteadiness affect the velocity and temperature profiles. The analysis is limited to two-dimensional, laminar flow without considering three-dimensional effects or experimental data.

1.6 Definition of Terms and Concept

Table 1.1 Definition of terms and concept

Terms and Concepts	Definition
Maxwell fluids	A type of fluid that acts like both viscosity and elasticity through relaxation time. (Hassan et al., 2025)
Magnetohydrodynamics (MHD)	A field of physics that studies how electrically conducting fluids like plasmas, metals, and ionized gases behave in magnetic fields (Salahuddin et al., 2024)
Radiation	Radiation is a way heat is transferred, especially in the development of advanced heat models, where its role becomes prominent at high temperature. (Sonam & Yadav, 2024)
Boundary layer	The boundary layer is a smooth fluid region near the surface where viscosity dominates and heat transfer occurs steadily. (Shah et al., 2025)
Viscous dissipation	The process where a fluid's movement creates heat because of its internal resistance to flow. (Sanderse & Trias, 2025)
Porous medium	A porous medium is a material with tiny spaces that allow fluids like water to pass through, useful in soil, irrigation, and industry. (Cajot et al., 2025)
Velocity slip	The non-zero fluid velocity at the solid boundary due to insufficient intermolecular interactions between the fluid and the surface. (Geraeilinezhad et al., 2023)

CHAPTER 2
LITERATURE REVIEW

2.1 Introduction

This chapter explores velocity slip in fluid dynamics and its effects on fluid behaviour. It highlights how slip influences Maxwell fluid flow over stretching surfaces, affecting boundary layers, magnetohydrodynamics (MHD), and heat transfer. Understanding these effects helps in analysing fluid movement and optimizing related applications.

2.2 Literature Review

In velocity slip the fluid is not ideal and slips past the rigid surface rather than sticking, and this changes the thickness of the boundary layers, the velocity profiles, and heat transfer mechanisms. Slip conditions are significant in non-Newtonian fluids such as Maxwell fluids, where when compared to Newtonian fluids, the fluids are viscoelastic and thus they interfere with transfer of momentum and heat energy in the flow. When a stretching surface is passed through, slip will influence shear stress, temperature profile and stability, yet fluid movement will also be influenced by magnetohydrodynamic (MHD) influence caused by external excitation such as magnetic fields. Velocity slip underlines the creation of realistic models of fluid and the estimation of heat and mass transfer behaviour and offers a deeper understanding of the growth process of boundary layer and flows in advanced systems.

Kezzar et al. (2023) did comprehensive research on the effect of velocity slip boundary conditions on converging/diverging channels on the MHD hybrid nanofluid flow. Taking into consideration their findings, an increment in the value of the velocity slip parameter minimizes the velocity gradient at the wall and, consequently, the skin friction coefficient by a large order. They also discovered that the gradients in wall temperature minimizes with more slip thus resulting to lower rate of heat transfer and an effective increase in the thickness of the thermal boundary. Along the same lines, Iqbal et al. (2024) focused on the unsteady flow of Cu nanofluid/EG over a stretching surface with a partial slip boundary condition that showed that with an increment in the velocity slip parameter, both skin friction coefficient and heat transfer rate diminish. The temperature gradient near the wall is reduced and the thermal boundary layer

thickens. The reduced near-wall velocity due to the diminished shear-effects also causes the reduced thickness of the thermal boundary layer.

Moreover, Sharma and Gandhi (2022) researched the impact of the ventilated slip on an unstable magnetohydrodynamic (MHD) mixed circulation stream to vertically protruding surface in a Darcy-Forchheimer porous background. In their boundary conditions they accounted one dimensionless velocity slip parameter to model partial fluid adherence to the wall. Their result by increasing the slip parameter is that the velocity gradient close to the wall will reduce and will result in a lesser skin friction coefficient. Moreover, the temperature gradient adjacent to the wall also suffers a reduction and the rate of heat transfer reduces, and the thermal boundary layer gets thicker. Its impact was quite pronounced in the presence of high magnetic fields and porous environments when the slip inhibited the backflow and increased the flow stability.

Furthermore, Olabode et al. (2021) have examined the unsteady Maxwell fluid flow in a stretching surface in detail, which included the impacts of the changeable transport characteristics and nonlinear convection. They have defined a slip parameter to explain the un-edged flow of the fluid that flows on the wall in hot porous areas. Findings show that the velocity gradient close to the wall is diminished by greater velocity slip parameter which results in smaller skin friction coefficient value. The gradient in the wall temperature also becomes lower and the rate of heat transfer drops along with a thicker thermal boundary layer. Such effects take precedent in strong magnetic field and changing viscosity where slip contributed stability of the flow and reduced resistance.

Next, Reddy and Goud (2025) investigated magnetohydrodynamic (MHD) heat and mass transfer flow through a porous medium over an exponentially stretching sheet with velocity slip impacts, suction, and thermal radiation impacts. It was shown that the higher the value of the slip parameter, the more the velocity near the wall was decreased and the lower the skin friction and that the thermal and the concentration boundary layers were modified. These results highlight the need to consider velocity slip in the modelling of MHD flows, especially in porous and thermally active systems that are used in industrial processes, polymer extrusion, cooling technologies, and biomedical applications.

Besides that, Shah et al. (2022) have also studied about the slip and radiative impact on magnetohydrodynamic (MHD) Maxwell nanofluid flow past an inclined stretching surface set in a porous medium. In their results, they pointed out that the increase in slip parameter decreased the skin friction and velocity near the wall, among other alterations to the thermal and concentration boundary layer. The implication of the study has highly emphasized that the velocity slip used together with the effects of the magnetic and the porous medium is of immense importance in controlling the flow resistance and the thermal control manipulation in the viscoelastic nanofluid flows. Such revelations are more so in the optimization of heat and mass transfer in advanced thermal engineering applications.

In addition, Kamran et al. (2025) employed a computational study to examine the unsteady flow of graphene Maxwell nanofluid past a linear, stretched sheet, whereby the impacts of particular slip conditions, magnetic fields, and thermal radiations were considered in the research study. They used a slip parameter of velocity in their boundary conditions to capture the partial adhesion of fluid at the wall and this case is very relevant in micro- and nanofluid systems. It was found that the increase of slip parameter caused decrease in near-wall velocity and skin friction and influenced the boundary layer thickness on temperature. It was pointed out in the study that slip velocity is an important issue related to managing flow and increasing heat transfer in addition to Maxwell fluid behaviour and nanoparticle effects. The above results highlight the significance of factoring-in of slip effects in modelling of non-Newtonian flows of nanofluids necessary to be used in thermal management and advanced material processing.

Not only that, Maraj et al. (2022) introduced the velocity slip impact on magnetohydrodynamic (MHD) mix nanofluid stream in a vertical rotating tube with thermal periodic limits. They found that as the slip parameter was increased, the velocities that were closer to the wall were also reduced and this meant less shear interaction and skin friction. This paper has also shown that the effects of the velocity slip had a huge impact on the thermal and momentum boundary layers more so when there deemed interactions between the nanoparticle and rotational effects. Such findings show the significance of the velocity slip in the understanding of proper flow behaviour and maximum heat transfer enhancement in hybrid nanofluid functionalities applied in industrial and thermal engineering.

Equally important, Vishwanatha et al. (2023) revealed the influences of three parameters, namely the velocity slip and stretching ratio, in addition to Maxwell nanofluid magnetohydrodynamic (MHD) rotating flow over a stretching and shrinking sheet. Their result indicates that the velocity slip parameter tends to decrease the velocity gradient at the vicinity of the wall owing to which it reduces the skin friction coefficient. Similarly, the temperature gradient, at the surface, decreases, which results in reduced heat transfer rate and an increased thermal boundary layer. Their findings confirmed the fact that the hike in the slip parameter brought about a decrease both along and across the flow direction. Also, based on Geraeilinezhad et al. (2023), the velocity slip was investigated in the flow of the pseudoplastic non-Newtonian fluid in microchannels. The gradient of the velocity reduces as the slip parameter becomes larger and reduces the coefficient of skin friction. The wall temperature gradient is also reduced which causes the reduced rate of heat transfer and marginally thicker heat boundary layer.

Additionally, Memon et al. (2024) and Krishna and Kumar (2024) also analysed the impact of velocity slip in nanofluid over stretching surface with magnetic and porous conditions. In their conclusions, they find that an increment in the velocity slip parameter decreases the velocity gradient close to the wall resulting to reduced skin friction with diminished fluid-surface interaction. The two studies also reported that, enhancing the velocity slip resulted in a reduction in temperature gradient at the wall that reduced the rate of heat transfer and the boundary layer thickness. In general, the findings indicate that slip boundary condition do play critical role in changing flow resistance and thermal transportation in different nanofluid model.

In summary, velocity slip has a significant impact on fluid flow, especially in MHD and Maxwell fluid models. Increasing the slip parameter reduces the velocity and temperature gradients near the wall, leading to lower skin friction and heat transfer rates. These effects are more noticeable in porous, magnetic, and thermally active systems. Overall, including slip conditions improves the accuracy of flow and heat transfer predictions in complex fluid applications.

CHAPTER 3
RESEARCH METHODOLOGY

3.1 Introduction

There are seven main steps in conducting this study. The seven steps are as shown below:

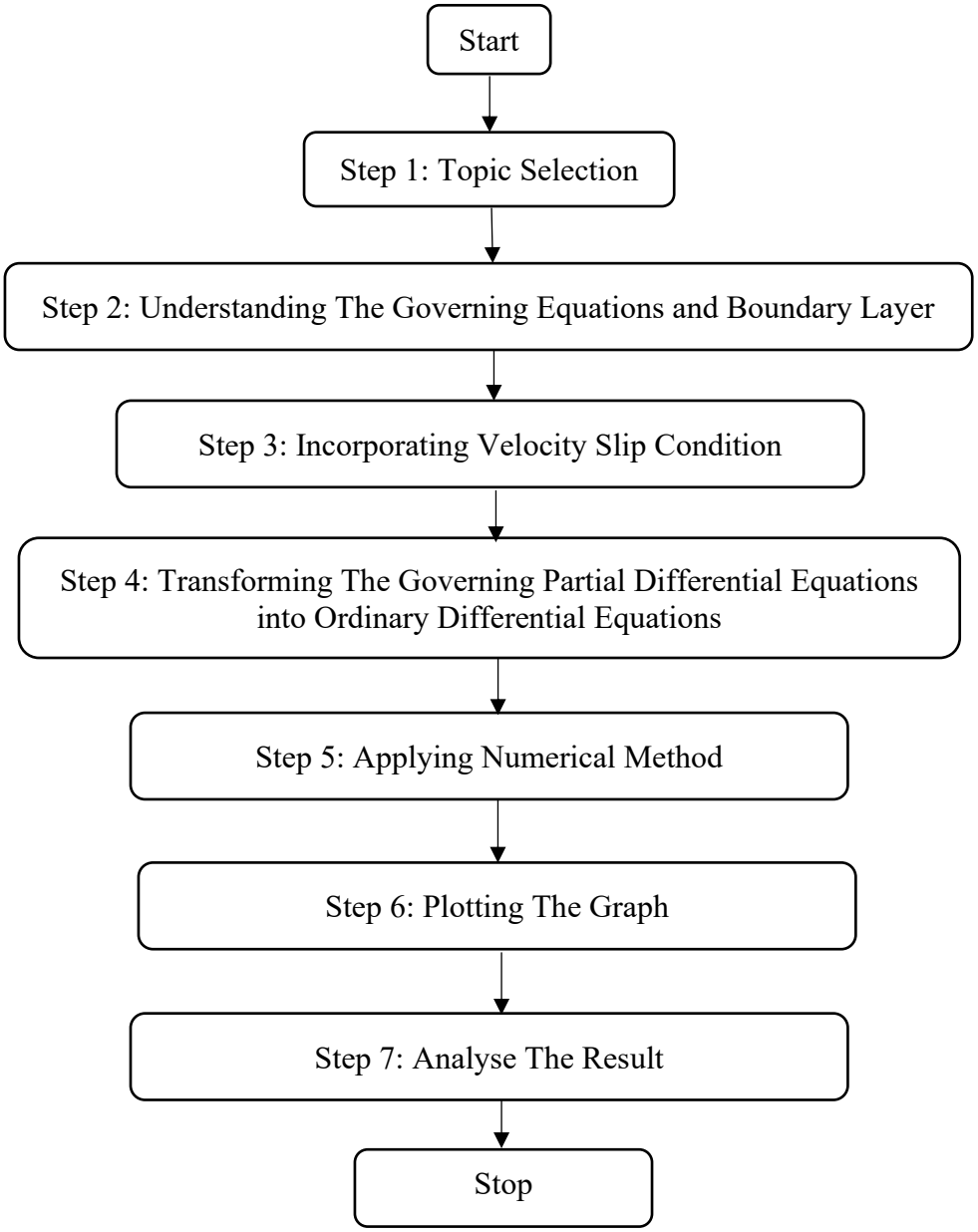

Figure 3.1 Research flow

3.1.1 Step 1: Topic Selection

The topic is selected based on an article by Sonam and Yadav (2024) entitled Numerical study of MHD Maxwell fluid flow from a stretching surface with radiation impact.

3.1.2 Step 2: Understanding the Governing Equation and Boundary Layer

The equations that involved in this article by Sonam and Yadav (2024) are continuity equation, momentum equation, and energy equation. The partial differential equations are as follows:

i. Continuity equation

$$\frac{\partial u}{\partial x}+\frac{\partial v}{\partial y}=0 \tag{3.1}$$

ii. Momentum equation

$$\frac{\partial u}{\partial t}+v\frac{\partial u}{\partial y}+u\frac{\partial u}{\partial x}=\frac{1}{\rho}\left(\frac{\partial \tau_{xx}}{\partial x}+\frac{\partial \tau_{xy}}{\partial y}\right)-\frac{v}{k}u-\frac{\sigma\beta^2 u}{\rho} \tag{3.2}$$

iii. Energy equation

$$\frac{\partial T}{\partial t}+v\frac{\partial T}{\partial y}+u\frac{\partial T}{\partial x}=\kappa\frac{\partial^2 T}{\partial y^2}+\frac{v}{c_p}\left(\frac{\partial u}{\partial y}\right)^2+\frac{\sigma\beta^2 u^2}{\rho c_p}-\frac{Q}{\rho c_p}(T_\infty-T)-\frac{1}{\rho c_p}\frac{\partial q_r}{\partial y} \tag{3.3}$$

where u and v are the fluid velocities along with the x and y axes, respectively. ρ is the liquid density, while τ_{xx} and τ_{xy} are the factors of the excess stress sensor. The permeability of the porous medium, $K(t)=\frac{K_0}{(1-\alpha t)}$, is assumed to change over time. The thermal diffusivity is $\kappa=\frac{k}{\rho c_p}$, with k as thermal conductivity and c_p as specific heat capacity. q_r is the radiative heat flux, v is the kinematic viscosity, σ is electrical conductivity, and B is the magnetic field strength squared. These parameters define the fluid's flow and heat transfer properties.

The boundary conditions are:

$$u = U_w(x,t), v = v_w(t), T = T_w(x,t), at\ y = 0, \tag{3.4}$$

$$u \to 0, T \to T_w, as\ y \to \infty \tag{3.5}$$

where $y = 0$, the fluid velocity and temperature match the wall, and as y→∞, the velocity becomes zero, and the temperature reaches the surrounding value.

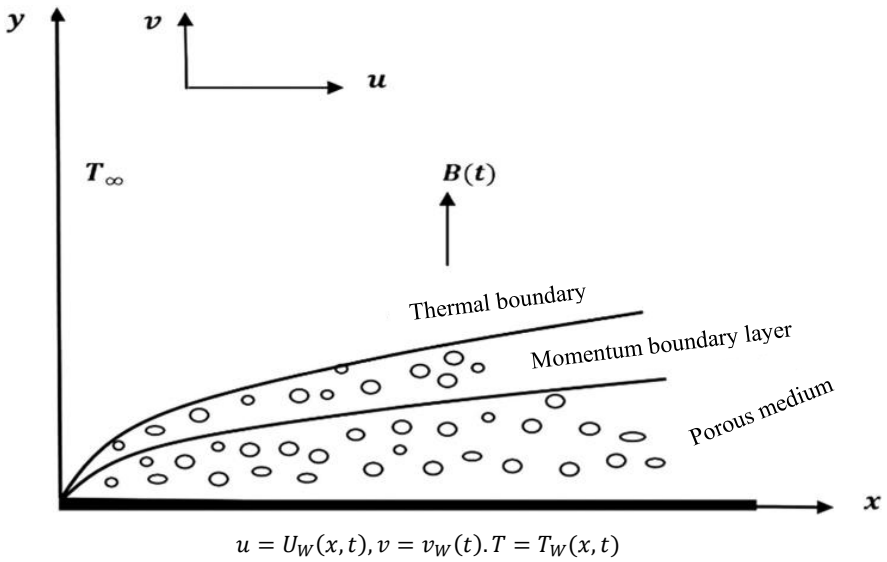

Figure 3.2 Physical model of fluid flow through stretching surface (Sonam & Yadav, 2024).

Figure 3.2 represents the flow and heat transfer of a Maxwell fluid over a stretching surface within a porous medium, representing unsteady boundary layer flow. Diagram illustrates momentum and thermal boundary layers with non-uniform surface velocity $u = U_w(x,t)$ and temperature $T = T_w(x,t)$, which vary with time and along the surface. Here, the ambient temperature is represented by T_∞ and the magnetic field $B(t)$ is taken to be applied perpendicular to the flow. The graph shows a satisfactory comparison with the assumptions of local thermal equilibrium between the porous surface and fluid.

3.1.3 Step 3: Incorporating Velocity Slip Condition

The velocity slip parameter is incorporated into the boundary condition to account for partial fluid movement at the wall. The slip condition is expressed as:

$$u - U_W = \ell \frac{\partial u}{\partial y} \tag{3.6}$$

where ℓ represents the characteristic slip length. Using the similarity transformation $\lambda = \ell \sqrt{\frac{c}{\nu(1-at)}}$, this condition transforms into:

$$f'(0) = 1 + \lambda f''(0) \tag{3.7}$$

This modified boundary condition replaces the traditional no-slip condition $f'(0) = 1$ and introduces the velocity slip parameter λ that quantifies the degree of slip at the surface. The complete boundary conditions now become:

At the surface (y=0):

$$f'(0) = 1 + \lambda f''(0), f(0) = S, \theta(0) = 1 \tag{3.8}$$

Far from the surface ($y \to \infty$**):**

$$f'(\infty) \to 0, \theta(\infty) \to 0 \tag{3.9}$$

The inclusion of λ modifies the flow behaviour near the surface, enabling a more accurate representation of nanoscale flows where full fluid adherence to the wall cannot be assumed.

3.1.4 Step 4: Transforming the Governing Partial Differential Equation into Ordinary Differential Equations

Based on Sonam and Yadav (2024), the PDEs are transformed into ODEs by using similarity transformations. The similarity transformations that is used is as follows:

$$\eta = y\sqrt{\frac{c}{v(1-at)}}\,, u = \frac{\partial \psi}{\partial y}, v = -\frac{\partial \psi}{\partial x}, \theta(\eta) = \frac{T - T_\infty}{T_w - T_\infty}, \psi(x) = \frac{x}{y}\eta v f(\eta) \qquad (3.10)$$

From Sonam and Yadav (2024), the substitution of these variables in the new governing equations, the ODEs that have been reduced from PDE are as follows:

i. Momentum equation

$$A\left(f' + \frac{\eta}{2}f''\right) + f'^2 - ff'' + \beta(f^2 f''' - 2ff'f'') = f''' - K_1 f' - Mf' \qquad (3.11)$$

ii. Energy equation

$$A\left(2\theta + \frac{\eta}{2}\theta'\right) = f\theta' - f'\theta + \frac{1}{Pr}\left(1 + \frac{4N}{3}\right)\theta'' + Ec\left(f''^2 + Mf'^2\right) + Q^*\theta \qquad (3.12)$$

The transformed boundary conditions are as follows:

$$\eta = 0, f(0) = S, f'(0) = 1 + \lambda\, f''(0), \theta(0) = 1 \qquad (3.13)$$

$$\eta \to \infty, f' \to 0, \theta \to 0 \qquad (3.14)$$

where prime denotes differentiation with respect to η, key parameters include $M = \frac{\sigma B_0^2}{\rho c_p}$ (magnetic parameter), $Q^* = \frac{Q_0}{\rho c_p c}$ (heat generation), $Pr = \frac{v\rho C_p}{k}$ (Prandtl number), $K_1 = \frac{v}{K_{0c}}$, and $A = \frac{a}{c}$. Additionally, $Ec = \frac{U_w}{c_p(T_w - T_\infty)}$. These parameters describe the fluid's thermal, magnetic, and flow properties, including heat generation, flow behaviour, and boundary effects.

3.1.5 Step 5: Numerical Method

The Runge-Kutta-Fehlberg (RKF45) method is applied to solve the equations, numerically. The momentum and energy along with their boundary conditions are solved numerically using Runge-Kutta-Fehlberg (RKF45) method. The obtained results are presented in tabular form and compared with those of Sonam and Yadav (2024) to verify accuracy. Key parameters such as the magnetic parameter (M), heat source parameter (Q^*), Prandtl number (Pr), porosity parameter (K_1), and Eckert number (Ec), which define the fluid's thermal, magnetic, and flow properties, are considered.

3.1.6 Step 6: Plotting the Graph

Plotting the graph is essential for observing the research outcome. The effects of different parameters are analysed, and conclusions can be drawn based on the graph analysis.

3.1.7 Step 7: Analyse the result

In comparing the results of this research paper and the findings of Sonam and Yadav (2024), it will be possible to analyse the numerical solutions and the graphs. This discussion can be used to arrive at the conclusions regarding the impacts of parameters like the velocity slip, magnetic parameter, Prandtl number, porosity parameter, suction or blowing parameter, Eckert number, heat source parameter and many more about the magnetohydrodynamic (MHD) boundary layer flow over a stretching surface in presence of radiation effects.

CHAPTER 4
IMPLEMENTATION

4.1 Introduction

This chapter focuses on the implementation step of this research. It involves three partial differential equations which were transformed into ordinary differential equations, which are continuity, momentum and energy. Additionally, velocity slip parameter is integrated into the boundary conditions.

4.2 Transformation of Partial Differential Equation into Ordinary Differential Equation

By considering the governing boundary layer equation from Sonam and Yadav (2024), the governing boundary layer equations are considered as follows:

i. Continuity equation

$$\frac{\partial u}{\partial x}+\frac{\partial v}{\partial y}=0$$

ii. Momentum equation

$$\frac{\partial u}{\partial t}+v\frac{\partial u}{\partial y}+u\frac{\partial u}{\partial x}=\frac{1}{\rho}\left(\frac{\partial \tau_{xx}}{\partial x}+\frac{\partial \tau_{xy}}{\partial y}\right)-\frac{v}{k}u-\frac{\sigma\beta^2 u}{\rho}$$

iii. Energy equation

$$\frac{\partial T}{\partial t}+v\frac{\partial T}{\partial y}+u\frac{\partial T}{\partial x}=\kappa\frac{\partial^2 T}{\partial y^2}+\frac{v}{c_p}\left(\frac{\partial u}{\partial y}\right)^2+\frac{\sigma\beta^2u^2}{\rho c_p}-\frac{Q}{\rho c_p}(T_\infty-T)-\frac{1}{\rho c_p}\frac{\partial q_r}{\partial y}$$

where u and v are the fluid velocities along with the x and y axes, respectively. ρ is the liquid density, while τ_{xx} and τ_{xy} are the factors of the excess stress sensor. The permeability of the porous medium, $K(t) = \frac{K_0}{(1-\alpha t)}$, is assumed to change over time. The thermal diffusivity is $\kappa = \frac{k}{\rho c_p}$, with k as thermal conductivity and c_p as specific heat capacity. q_r is the radiative heat flux, v is the kinematic viscosity, σ is electrical conductivity, and B is the magnetic field strength squared. These parameters define the fluid's flow and heat transfer properties.

The boundary condition is given by:

$$u = U_w(x,t), v = v_w(t), T = T_w(x,t), at\ y = 0, \tag{4.1}$$

$$u \to 0, T \to T_w, as\ y \to \infty \tag{4.2}$$

The non-uniform velocity, U_w and velocity of suction is defined as

$$U_W(x,t) = \frac{cx}{(1-at)}, V_W = \frac{-V_0}{\sqrt{1-at}} \tag{4.3}$$

where $a > 0$, $b > 0$, and $c > 0$ are constants which are a controls unsteadiness, b adjusts surface temperature variation, and c sets the stretching rate of the surface. The slip condition is expressed as:

$$u - U_w = \ell \frac{\partial u}{\partial y}, \lambda = \ell \sqrt{\frac{c}{v(1-at)}} \tag{4.4}$$

where ℓ represents the characteristic distance beyond the surface where the extrapolated fluid velocity matches the wall velocity.

The surface temperature, $T_W(x,t)$ is given by

$$T_W(x,t) = T_\infty + \frac{bx}{(1-at)^2} \tag{4.5}$$

The similarity variables used in the transformation is as follows:

$$\eta = y\sqrt{\frac{c}{v(1-at)}}, \theta(\eta) = \frac{T - T_\infty}{T_w - T_\infty}, \psi(x) = \frac{x}{y}\eta v f(\eta) \tag{4.6}$$

The stream function, ψ is defined as $u = \partial\psi/\partial y$ and $v = -\partial\psi/\partial x$, while the similarity variable is defined as η.

From the similarity variable η in (4.8), y can be describe as

$$y = \eta\sqrt{\frac{v(1-at)}{c}}. \tag{4.7}$$

Substituting y from (4.10) into η in (4.9), the derivative of η with respect to x, y and t are:

$$\frac{\partial\eta}{\partial x} = \frac{\partial}{\partial x}\left[y\sqrt{\frac{c}{v(1-at)}}\right],$$

$$= 0 \tag{4.8}$$

$$\frac{\partial\eta}{\partial y} = \frac{\partial}{\partial y}\left[y\sqrt{\frac{c}{v(1-at)}}\right],$$

$$= \sqrt{\frac{c}{v(1-at)}}. \tag{4.9}$$

$$\frac{\partial\eta}{\partial t} = \frac{\partial}{\partial t}\left[y\sqrt{\frac{c}{v(1-at)}}\right],$$

$$= y\sqrt{\frac{c}{v}}.\left(-\frac{1}{2}\right).(1-at)^{\frac{3}{2}}.(-a)$$

$$= \sqrt{\frac{c}{v}}.\frac{ya}{2(1-at)^{\frac{3}{2}}}. \tag{4.10}$$

To obtain $u = \partial\psi/\partial y$ and $v = -\partial\psi/\partial x$, the derivative of ψ from (4.9) with respect to x and y are:

$$u = \frac{\partial \psi}{\partial y},$$

$$= \frac{\partial}{\partial y}\left[y\sqrt{\frac{cv}{(1-at)}}xf(\eta)\right],$$

$$= \sqrt{\frac{cv}{1-at}}.x.\frac{\partial f(\eta)}{\partial \eta}.\frac{\partial \eta}{\partial y} = \sqrt{\frac{cv}{1-at}}.x.f'(\eta).\sqrt{\frac{c}{v(1-at)}},$$

$$= \frac{cx}{1-at}f'(\eta). \tag{4.11}$$

$$v = -\frac{\partial \psi}{\partial x},$$

$$= \frac{\partial}{\partial x}\left[\sqrt{\frac{cv}{(1-at)}}xf(\eta)\right],$$

$$= -\left[\sqrt{\frac{cv}{1-at}}.x.\frac{\partial f(\eta)}{\partial \eta}.\frac{\partial \eta}{\partial y} + \sqrt{\frac{cv}{1-at}}.f(\eta)\right],$$

$$= -\left[\sqrt{\frac{cv}{1-at}}.\ x\ .f'(\eta).(0) + \sqrt{\frac{cv}{(1-at)}}.f(\eta)\right],$$

$$= -\sqrt{\frac{cv}{1-at}}f(\eta). \tag{4.12}$$

The derivative of u from (4.11) with respect to x, the first and second derivative with respect to y and t are:

$$\frac{\partial u}{\partial x} = \frac{\partial}{\partial x}\left[\frac{cx}{(1-at)}f'(\eta)\right],$$

$$= \frac{cx}{1-at}\cdot\frac{\partial f'(\eta)}{\partial \eta}\cdot\frac{\partial \eta}{\partial y} + \frac{c}{1-at}f'(\eta),$$

$$= \frac{cx}{1-at}\cdot(\eta)\cdot(0) + \frac{c}{1-at}f'(\eta)$$

$$= \frac{c}{1-at} f'(\eta). \tag{4.13}$$

$$\frac{\partial u}{\partial y} = \frac{\partial}{\partial y}\left[\frac{cx}{(1-at)} f'(\eta)\right],$$

$$= \frac{cx}{1-at} \cdot \frac{\partial f'(\eta)}{\partial \eta} \cdot \frac{\partial \eta}{\partial y},$$

$$= \frac{cx}{1-at} \cdot f''(\eta) \cdot \sqrt{\frac{c}{v(1-at)}},$$

$$= \frac{c^{\frac{3}{2}}x}{\sqrt{v}(1-at)^{\frac{3}{2}}} f''(\eta). \tag{4.14}$$

$$\frac{\partial^2 u}{\partial y^2} = \frac{\partial}{\partial y}\left[\frac{c^{\frac{3}{2}}x}{\sqrt{v}(1-at)^{\frac{3}{2}}} f''(\eta)\right],$$

$$= \frac{c^{\frac{3}{2}}x}{\sqrt{v}(1-at)^{\frac{3}{2}}} \cdot \frac{\partial f''(\eta)}{\partial \eta} \cdot \frac{\partial \eta}{\partial y},$$

$$= \frac{c^{\frac{3}{2}}x}{\sqrt{v}(1-at)^{\frac{3}{2}}} \cdot (\eta) \cdot \sqrt{\frac{c}{v(1-at)}},$$

$$= \frac{c^2 x}{v(1-at)^2} f'''(\eta). \tag{4.15}$$

$$\frac{\partial u}{\partial t} = \frac{\partial}{\partial t}\left[\frac{cx}{(1-at)} f''(\eta)\right],$$

$$= \frac{cx}{1-at} \cdot \frac{\partial f'(\eta)}{\partial \eta} \cdot \frac{\partial \eta}{\partial y} + (-1)\left(\frac{cx}{(1-at)^2}\right)(-a)\left(f'(\eta)\right),$$

$$= \frac{cx}{1-at} \cdot f''(\eta) \cdot \sqrt{\frac{c}{v}} \cdot \frac{ya}{2(1-at)^{\frac{3}{2}}} + \frac{acx}{(1-at)^2} f'(\eta),$$

$$= \frac{yac^{\frac{3}{2}}x}{2v^{\frac{1}{2}}(1-at)^{\frac{5}{2}}} f''(\eta) + \frac{acx}{(1-at)^2} f'(\eta). \tag{4.16}$$

$$\frac{\partial^2 u}{\partial x^2} = \frac{\partial}{\partial x}\left[\frac{c}{1-at} f'(\eta)\right],$$

$$= \frac{c}{1-at} \cdot \frac{\partial f''(\eta)}{\partial \eta} \cdot \frac{\partial \eta}{\partial x} = \frac{c}{1-at} \cdot f'''(\eta) \cdot \frac{\partial \eta}{\partial x},$$

$$= \frac{c}{1-at} \cdot f'''(\eta) \cdot (0),$$

$$= 0. \tag{4.17}$$

$$\frac{\partial^2 u}{\partial x \partial y} = \frac{\partial}{\partial y}\left[\frac{c}{1-at} f'(\eta)\right],$$

$$= \frac{c}{1-at} \cdot \frac{\partial}{\partial y} f'(\eta) = \frac{c}{1-at} \cdot f''(\eta) \cdot \frac{\partial \eta}{\partial y},$$

$$= \frac{c}{1-at} \cdot f''(\eta) \cdot \sqrt{\frac{c}{v(1-at)}},$$

$$= \frac{c^{\frac{3}{2}}}{\sqrt{v}\,(1-at)^{\frac{3}{2}}} f''(\eta). \tag{4.18}$$

The derivative of v from (4.12) with respect to y is:

$$\frac{\partial v}{\partial y} = \frac{\partial}{\partial y}\left[-\sqrt{\frac{cv}{(1-at)}} f(\eta)\right],$$

$$= -\sqrt{\frac{cv}{1-at}} \cdot \frac{\partial f(\eta)}{\partial \eta} \cdot \frac{\partial \eta}{\partial y},$$

$$= -\sqrt{\frac{cv}{1-at}} \cdot f'(\eta) \cdot \sqrt{\frac{c}{v(1-at)}},$$

$$= -\frac{c}{1-at}\, f'(\eta). \tag{4.19}$$

Furthermore, the surface temperature, T_W from (4.5) are substituted into the similarity variable T from (4.9) to obtain a new equation:

$$T = T_\infty + (T_W - T_\infty)\theta(\eta),$$

$$= T_\infty + \left[T_\infty + \frac{bx}{(1-\partial t)^2} - T_\infty\right]\theta(\eta),$$

$$= T_\infty + \frac{bx}{(1-at)^2}\theta(\eta). \tag{4.20}$$

The derivative of T from (4.20) with respect to x, the first and second derivative with respect to y and t are:

$$\frac{\partial T}{\partial x} = \frac{\partial}{\partial x}\left[T_\infty + \frac{bx}{(1-at)^2}\theta(\eta)\right],$$

$$= 0 + \left(\frac{b}{(1-at)^2}\right)\theta(\eta) - \frac{bx}{(1-at)^2}\cdot\frac{\partial\theta(\eta)}{\partial\eta}\cdot\frac{\partial\eta}{\partial x}$$

$$= 0 + \left(\frac{b}{(1-at)^2}\right)\theta(\eta) - \frac{bx}{(1-at)^2}\cdot\theta''(\eta)\cdot(0)$$

$$= \frac{b}{(1-at)^2}\cdot\theta(\eta). \tag{4.21}$$

$$\frac{\partial T}{\partial y} = \frac{\partial}{\partial y}\left[T_\infty + \frac{bx}{(1-at)^2}\theta(\eta)\right]$$

$$= 0 + \left(\frac{bx}{(1-at)^2}\right)\cdot\frac{\partial\theta(\eta)}{\partial\eta}\cdot\frac{\partial\eta}{\partial y}$$

$$= \frac{bx}{(1-at)^2}\cdot\theta'(\eta)\cdot\sqrt{\frac{c}{v(1-at)}},$$

$$= \frac{bx\sqrt{c}}{\sqrt{v}(1-at)^{\frac{5}{2}}}\cdot\theta'(\eta). \tag{4.22}$$

$$\frac{\partial^2 T}{\partial y^2} = \frac{\partial}{\partial y}\left[\frac{bx}{(1-at)^2}\cdot\theta'(\eta)\cdot\sqrt{\frac{c}{v(1-at)}}\right],$$

$$= \frac{\partial}{\partial y}\left[\frac{bx\sqrt{c}}{\sqrt{v}(1-at)^{\frac{5}{2}}}\cdot\theta'(\eta)\right],$$

$$= \left(\frac{bx\sqrt{c}}{\sqrt{v}(1-at)^{\frac{5}{2}}}\right)\cdot\frac{\partial\theta'(\eta)}{\partial\eta}\cdot\frac{\partial\eta}{\partial y},$$

$$= \frac{bx\sqrt{c}}{\sqrt{v}(1-at)^{\frac{5}{2}}}\cdot\theta''(\eta)\cdot\sqrt{\frac{c}{v(1-at)}},$$

$$= \frac{bxc}{v(1-at)^3}\cdot\theta''(\eta). \tag{4.23}$$

$$\frac{\partial T}{\partial t} = \frac{\partial}{\partial t}\left[T_\infty + \frac{bx}{(1-at)^2}\cdot\theta(\eta)\right]$$

$$= 0 + \frac{\partial}{\partial t}\left[\frac{bx}{(1-at)^2}\theta(\eta)\right]$$

$$= \theta(\eta)\cdot(-2)\left[\frac{bx}{(1-at)^3}\right](-a) + \left(\frac{bx}{(1-at)^3}\right)\cdot\frac{\partial\theta(\eta)}{\partial\eta}\cdot\frac{\partial n}{\partial t}$$

$$= \theta(\eta)\cdot 2\alpha\cdot\left(\frac{bx}{(1-at)^3}\right) + \left(\frac{bx}{(1-at)^3}\right)\cdot\theta'(\eta)\cdot\eta$$

$$= \frac{2abx}{(1-at)^3}\theta(\eta) + \frac{abx\eta}{(1-at)^3}\theta'(\eta) \tag{4.24}$$

4.2.1 Continuity equation

The equation (4.13) and (4.19) are substituted into the continuity equation in (3.1)

$$\frac{\partial u}{\partial x} + \frac{\partial v}{\partial y} = 0,$$

$$\frac{c}{1-at}f'(\eta) + \left(-\frac{c}{1-at}f'(\eta)\right) = 0. \tag{4.25}$$

4.2.2 Momentum equation

Equation (4.3), (4.11), (4.12), (4.13), (4.14), (4.15), (4.16), (4.17) and (4.18) are substituted into the momentum equation in (3.2)

$$\frac{\partial u}{\partial t}+v\frac{\partial u}{\partial y}+u\frac{\partial u}{\partial x}=\frac{1}{\rho}\left(\frac{\partial \tau_{xx}}{\partial x}+\frac{\partial \tau_{xy}}{\partial y}\right)-\frac{v}{K}u-\frac{\sigma\beta^2 u}{\rho}$$

where the momentum equation can be simplified by utilizing the boundary layer principle

$$\frac{\partial u}{\partial t}+v\frac{\partial u}{\partial y}+u\frac{\partial u}{\partial x}=v\frac{\partial^2 u}{\partial y}-\lambda\left(u^2\frac{\partial^2 u}{\partial x^2}+2uv\frac{\partial^2 u}{\partial x\partial y}+v^2\frac{\partial^2 u}{\partial y^2}\right)-\frac{v}{K}u-\frac{\sigma B^2 u}{\rho}$$

$$\left(\frac{yac^{\frac{3}{2}}x}{2v^{\frac{1}{2}}(1-at)^{\frac{5}{2}}}f''(\eta)+\frac{acx}{(1-at)^2}f'(\eta)\right)$$

$$+\left(-\sqrt{\frac{cv}{1-at}}f(\eta)\right)\left(\frac{c^{\frac{3}{2}}x}{\sqrt{v}(1-at)^{\frac{3}{2}}}f''(\eta)\right)$$

$$+\left(\frac{cx}{1-at}f'(\eta)\right)\left(\frac{c}{1-at}f'(\eta)\right)$$

$$=v\left(\frac{c^2x}{v(1-at)^2}f'''(\eta)\right)-\lambda[\left(\frac{cx}{1-at}f'(\eta)\right)^2(0)$$

$$+2\left(\frac{cx}{1-at}f'(\eta)\right)\left(-\sqrt{\frac{cv}{1-at}}f(\eta)\right)\left(\frac{c^{\frac{3}{2}}}{\sqrt{v}\,(1-at)^{\frac{3}{2}}}f''(\eta)\right)$$

$$+\left(-\sqrt{\frac{cv}{1-at}}f(\eta)\right)^2]-\left(\frac{v}{K}\right)\left(\frac{cx}{1-at}f'(\eta)\right)$$

$$-\left(\frac{\sigma\beta^2}{\rho}\right)\left(\frac{cx}{1-at}f'(\eta)\right) \qquad (4.26)$$

$$\left(\frac{yac^{\frac{3}{2}}x}{2v^{\frac{1}{2}}(1-at)^{\frac{5}{2}}}f''(\eta)+\frac{acx}{(1-at)^2}f'(\eta)\right)$$

$$+\left(-\sqrt{\frac{cv}{1-at}}f(\eta)\right)\left(\frac{c^{\frac{3}{2}}x}{\sqrt{v}(1-at)^{\frac{3}{2}}}f''(\eta)\right)+\left(\frac{cx}{1-at}f'(\eta)\right)$$

$$=\left(\frac{c^2x}{(1-at)^2}f'''(\eta)\right)-\lambda\left(-2\left(\frac{c^3x}{(1-at)^3}f(\eta)f'(\eta)f'''(\eta)\right)\right)$$

$$+\left(\frac{c^3x}{(1-at)^3}f(\eta)^2f'''(\eta)\right)-\left(\frac{v}{K}\right)\left(\frac{cx}{1-at}f'(\eta)\right)$$

$$-\left(\frac{\sigma\beta^2}{\rho}\right)\left(\frac{cx}{1-at}f'(\eta)\right) \tag{4.27}$$

$$\left(\frac{acx}{(1-at)^2}\left(\frac{c^{\frac{1}{2}}y}{2v^{\frac{1}{2}}(1-at)^{\frac{5}{2}}}f''(\eta)+f'(\eta)\right)\right)$$

$$+\left(-\sqrt{\frac{cv}{1-at}}f(\eta)\right)\left(\frac{c^{\frac{3}{2}}x}{\sqrt{v}(1-at)^{\frac{3}{2}}}f''(\eta)\right)+\left(\frac{cx}{1-at}f'(\eta)\right)$$

$$=\left(\frac{c^2x}{(1-at)^2}f'''(\eta)\right)-\lambda\left(-2\left(\frac{c^3x}{(1-at)^3}f(\eta)f'(\eta)f'''(\eta)\right)\right)$$

$$+\left(\frac{c^3x}{(1-at)^3}f(\eta)^2f'''(\eta)\right)-\left(\frac{v}{K}\right)\left(\frac{cx}{1-at}f'(\eta)\right)$$

$$-\left(\frac{\sigma\beta^2}{\rho}\right)\left(\frac{cx}{1-at}f'(\eta)\right) \tag{4.28}$$

After substituting expressions for u, v and all their relevant derivatives, the momentum equation becomes:

$$\frac{acx}{(1-at)^2}\left(\frac{\eta}{2}f'' + f'\right) + \frac{c^2x}{(1-at)^2}((f')^2 - ff'')$$

$$+\beta\left(\frac{c^3x}{(1-at)^3}f^2f''' - \frac{2c^3x}{(1-at)^3}ff'f''\right)$$

$$= \frac{c^3x}{(1-at)^3}f''' - \frac{v}{K_1}\cdot\frac{cx}{1-at}f' - \frac{\sigma\beta^2}{\rho}\cdot\frac{cx}{1-at}f' \qquad (4.29)$$

Dividing the equation by $c^3x/(1-at)^3$, the equation transforms into:

$$\frac{a}{c}\left(\frac{\eta}{2}f'' + f'\right) + (f')^2 - ff'' + \beta(f^2f''' + 2ff'f'') = f''' - K_1f' - Mf' \qquad (4.30)$$

By substituting $A=a/c$ and $M=(\sigma\beta^2)/\rho\cdot(1-at)/c$, the momentum equation is simplified into:

$$A\left(f' + \frac{\eta}{2}f''\right) + f'^2 - ff'' + \beta(f^2f''' + 2ff'f'') = f''' - K_1f' - Mf' \qquad (4.31)$$

4.2.3 Energy equation

The value of radiative heat flux, $q_r = -(\frac{16\sigma^*T_\infty^3}{3\rho c_p k^*})\cdot(\partial T/\partial y)$ is substituted into energy equation in (3.3)

$$\frac{\partial T}{\partial t} + v\frac{\partial T}{\partial y} + u\frac{\partial T}{\partial x} = \left(\kappa + \frac{16\sigma^*T_\infty^3}{3\rho c_p k^*}\right)\frac{\partial^2 T}{\partial y^2} + \frac{v}{c_p}\left(\frac{\partial u}{\partial y}\right)^2 + \frac{\sigma\beta^2u^2}{\rho c_p} - \frac{Q}{\rho c_p}(T_\infty - T) \qquad (4.32)$$

Equation (4.21), (4.22), (4.23) and (4.24) are substituted into the energy equation in (3.3)

$$\frac{2abx}{(1-at)^3}\theta(\eta) + \frac{abx\eta}{2(1-at)^3}\theta'(\eta)$$

$$+\left(-\sqrt{\frac{cv}{1-at}}f(\eta)\right)\left(\frac{bx\sqrt{c}}{\sqrt{v}(1-at)^{\frac{5}{2}}}\cdot\theta'(\eta)\right)$$

$$+\left(\frac{cx}{1-at}\,f'(\eta)\right)\left(\frac{b}{(1-at)^2}\cdot\theta(\eta)\right)$$

$$=\left(\kappa+\frac{16\sigma^*T_\infty^3}{3\rho c_p k^*}\right)\frac{bcx}{v(1-at)^3}\cdot\theta''(\eta)+\frac{v}{c_p}\left(\frac{c^{\frac{3}{2}}x}{\sqrt{v}(1-at)^{\frac{3}{2}}}f''(\eta)\right)$$

$$+\frac{\sigma\beta^2}{\rho c_p}\left(\frac{cx}{1-at}f'(\eta)\right)^2-\frac{Q}{\rho c_p}\left(\frac{bx}{(1-at)^2}\theta(\eta)\right) \tag{4.33}$$

$$\frac{2abx}{(1-at)^3}\theta(\eta)+\frac{abx\eta}{2(1-at)^3}\theta'(\eta)$$

$$-\left(\frac{bcx}{(1-at)^3}f(\eta)\theta'(\eta)\right)+\left(\frac{bcx}{(1-at)^3}f'(\eta)\theta(\eta)\right)$$

$$=\left(\kappa+\frac{16\sigma^*T_\infty^3}{3\rho c_p k^*}\right)\frac{bcx}{v(1-at)^3}\cdot\theta''(\eta)+\frac{c^3x^2}{vc_p(1-at)^3}\left(f''(\eta)\right)^2$$

$$+\frac{\sigma\beta^2c^2x^2}{\rho c_p(1-at)^2}\left(f'(\eta)\right)^2-\frac{Q_0bx}{\rho c_p(1-at)^3}\theta(\eta) \tag{4.34}$$

Multiplying the equation by $(1\text{-}at)^3/bx$ to eliminate $(1\text{-}at)$ and x-dependence, the equation becomes

$$2a\theta+\frac{a\eta}{2}\theta'+cf'\theta-cf\theta'$$

$$=\left(\frac{c}{v}\right)\left(\kappa+\frac{16\sigma^*T_\infty^3}{3\rho c_p k^*}\right)\theta''+\left(\frac{c^3x^2}{vc_p(1-at)^3}\right)(f'')^2$$

$$+\frac{\sigma B^2c^2x^2}{\rho c_p(1-at)^2}(f')^2+\frac{Q_0v}{\rho c_p}\theta \tag{4.35}$$

Then dividing through by c and group the terms

$$\frac{a}{c}\left(2\theta+\frac{\eta}{2}\theta'\right)+f'\theta-f\theta'$$

$$=\left(\frac{\kappa}{v}\right)\left(1+\frac{16\sigma^*T_\infty^3}{3\rho c_p k^*}\right)\theta''+\left(\frac{c^2x^2}{vc_p(1-at)^3}\right)(f'')^2$$

$$+\frac{\sigma \mathrm{B}^2 \mathrm{c} x^2}{\rho c_p (1-at)^2}(f')^2 + \frac{Q_0}{\rho c_p c}\theta \tag{4.36}$$

Rearranging the energy equation and substituting $A=a/c$, $\kappa=k/pc_p$, $Pr=v/k$ and $Q*=Q_0/pc_pc$, it becomes

$$A\left(2\theta + \frac{\eta}{2}\theta'\right) + f'\theta - f\theta'$$

$$= \left(\frac{1}{Pr}\right)\left(1 + \frac{16\sigma^* T_\infty^3}{3\kappa k^*}\right)\theta'' + \left(\frac{c^2 x^2}{c_p(1-at)^3}\right)(f'')^2$$

$$+\frac{\sigma \mathrm{B}^2 \mathrm{c} x^2}{\rho c_p (1-at)^2}(f')^2 + Q^*\,\theta \tag{4.37}$$

For $B = B_0/(1\text{-at})$

$$\left[\left(\frac{c^2 x^2}{c_p(1-at)^3}\right)(f'')^2 + \frac{\sigma B_0^2 \mathrm{c} x^2}{\rho c_p (1-at)^3}(f')^2\right] \times \frac{(1-at)^3}{bx}$$
$$= \frac{c^2 x}{b c_p}\left[(f'')^2 + \frac{\sigma B_0^2}{\rho c_p}(f')^2\right] \tag{4.38}$$

Substituting $N=4\sigma^* T_\infty^3/\kappa k^*$, $Ec=c^2x/bc_p$ and $M = \sigma B_0^2/\rho c_p$ and rearranging, the equation becomes

$$A\left(2\theta + \frac{\eta}{2}\theta'\right) = f\theta' - f'\theta + \frac{1}{Pr}\left(1 + \frac{4\mathrm{N}}{3}\right)\theta'' + Ec\left(f''^2 + Mf'^2\right) + Q^*\,\theta \tag{4.39}$$

4.2.4 Boundary conditions

4.2.4.1 Boundary conditions as y = 0

When y = 0:

$$\eta = y\sqrt{\frac{c}{v(1-at)}},$$

$$= (0)\sqrt{\frac{c}{v(1-at)}},$$

$$= 0. \tag{4.40}$$

Equation (4.3), (4.4), (4.11), and (4.14) are substituted into u in (4.1) then the equation becomes

$$\frac{cx}{1-at}f'(\eta) - \frac{cx}{1-at} = \ell\left(\frac{c^{\frac{3}{2}}x}{\sqrt{v}(1-at)^{\frac{3}{2}}}f''(\eta)\right)$$

$$\frac{cx}{1-at}(f'(\eta)-1) = \ell\left(\frac{c^{\frac{3}{2}}x}{\sqrt{v}(1-at)^{\frac{3}{2}}}f''(\eta)\right) \tag{4.41}$$

Dividing both sides by *cx/1-at* and simplify the equation, the equation becomes

$$f'(\eta) - 1 = \ell\left(\sqrt{\frac{c}{v(1-at)}}f''(\eta)\right) \tag{4.42}$$

Substituting velocity slip parameter, $\lambda = \ell\sqrt{c\ /\mathrm{v}(1-\mathrm{at})}$ and substituting η = 0, the equation becomes

$$f'(\eta) - 1 = \lambda\, f''(\eta)$$

$$f'(0) = 1 + \lambda\, f''(0) \tag{4.43}$$

The boundary condition for v from (4.12) is $v(\eta) = v_w$. Thus, it can be written as

$$-\sqrt{\frac{cv}{1-at}}f(\eta) = \frac{-V_0}{\sqrt{1-at}} \tag{4.44}$$

Eliminating $\sqrt{(1\ -\ \alpha\mathrm{t})}$ and substituting η = 0, the equation become

$$-\sqrt{cv}f(0) = -V_0 \tag{4.45}$$

Solving for $f(0)$

$$f(0) = \frac{V_0}{\sqrt{cv}} = S$$

$$f(0) = S \tag{4.46}$$

Substituting (4.5), (4.20), and (4.22) into T in (4.1), the equation becomes

$$T_\infty + \frac{bx}{(1-at)^2} = T_\infty + \frac{bx}{(1-at)^2}\theta(\eta) \tag{4.47}$$

Subtracting T_∞ from both sides

$$\frac{bx}{(1-at)^2} = \frac{bx}{(1-at)^2}\theta(\eta) \tag{4.48}$$

Dividing both sides by $bx/(1-at)^2$ and set $\eta = 0$

$$1 = \theta(0)$$

$$\theta(0) = 1 \tag{4.49}$$

Hence the boundary condition when $y = 0$ are

$$f'(0) = 1 + \lambda\, f''(0), f(0) = S, \theta(0) = 1. \tag{4.50}$$

4.2.4.2 Boundary condition as y → ∞:

When y → ∞:

$$\eta = y\sqrt{\frac{c}{v(1-at)}},$$

$$= (\infty)\sqrt{\frac{c}{v(1-at)}},$$

$$= \infty. \tag{4.51}$$

As u → 0, the equation (4.3) and (4.11) is substituted into (4.2)

$$\frac{cx}{1-at} f'(\eta) \to 0. \tag{4.52}$$

The equation is rearranged and become

$$f'(\eta) \to 0 \tag{4.53}$$

As $T \rightarrow Tw$, the similarity transformation from (4.9) is substituted into the equation and become

$$T \rightarrow T_\infty + (T_w - T_\infty)\theta(\eta) \tag{4.54}$$

Rearranging the equation and subtracting T_∞ from both sides of the equation and become

$$T - T_\infty \rightarrow (T_w - T_\infty)\theta(\eta) \tag{4.55}$$

As $T \rightarrow T_\infty$, the left-hand side approaches zero

$$(T_w - T_\infty)\theta(\eta) \rightarrow 0 \tag{4.56}$$

Since $T_w \neq T_\infty$, we can divide both sides by $T_w - T_\infty$:

$$\theta(\eta) \rightarrow 0 \tag{4.57}$$

Hence, the boundary conditions as $y \rightarrow \infty$ are

$$f'(\infty) \rightarrow 0, \theta(\infty) \rightarrow 0 \tag{4.58}$$

4.2.4.3 Skin friction

The Reynolds number can be defined as

$$Re_x = \frac{U_w x}{v},$$

$$= \frac{cx}{(1-at)}\frac{x}{v},$$

$$= \frac{cx^2}{v(1-at)}. \tag{4.59}$$

The shear stress can be represented as $\tau_w = \mu(\partial u/\partial y)_{y=0}$. Hence, the skin friction coefficient, C_{f_x} can be written as

$$C_f = \frac{\tau_w}{\rho U_w^2},$$

$$= \frac{\mu\left(\frac{\partial u}{\partial y}\right)_{y=0}}{\rho U_w^2},$$

$$= \frac{\mu \cdot \frac{cx}{1-at} \cdot f''(\eta) \cdot \sqrt{\frac{c}{v(1-at)}}}{\rho U_w^2} \tag{4.60}$$

Using kinematic viscosity where $v = \mu/\rho$, the skin friction is simplified into

$$C_{f_x} = \frac{v \cdot \frac{cx}{1-at} \cdot f''(\eta) \cdot \sqrt{\frac{c}{v(1-at)}}}{U_w^2} \tag{4.61}$$

Substituting (4.3) and simplifying the equation, it become

$$C_{f_x} = \frac{v \cdot \frac{cx}{1-at} \cdot f''(0) \cdot \sqrt{\frac{c}{v(1-at)}}}{\left(\frac{cx}{(1-at)}\right)^2}$$

$$= v \cdot \frac{cx}{1-at} \cdot \sqrt{\frac{c}{v(1-at)}} \cdot \left(\frac{(1-at)}{cx}\right)^2 \cdot f''(0)$$

$$= \sqrt{v} \cdot \frac{c^{\frac{3}{2}} x \sqrt{(1-at)}}{c^2 x^2} f''(0)$$

$$= \sqrt{v} \cdot \frac{\sqrt{(1-at)}}{\sqrt{c}x} f''(0) \tag{4.62}$$

Rearranging the equation where $Re_x = U_w x / v$

$$Re_x = \frac{U_w x}{v} = \frac{cx^2}{v(1-at)}$$

$$\sqrt{v} = \frac{x\sqrt{c}}{\sqrt{Re_x(1-at)}} \tag{4.63}$$

Then substituting $\sqrt{v}$ into C_{f_x}

$$C_{f_x} = \frac{x\sqrt{c}}{\sqrt{Re_x(1-at)}} \cdot \frac{\sqrt{(1-at)}}{\sqrt{c}x} f''(0)$$

$$C_{f_x} = \frac{f''(0)}{\sqrt{Re_x}}$$

$$C_{f_x}\sqrt{Re_x} = f''(0) \tag{4.64}$$

4.2.4.4 Nusselt Number, Nu_x

The surface heat flux,q_w can be defined as

$$q_w = -x\left(\frac{\partial T}{\partial y}\right)_{y=0},$$

$$= -x(T_w - T_\infty)\theta'(\eta)\sqrt{\frac{U}{vx}} \tag{4.65}$$

Substituting (4.65) into the equation, it becomes

$$\mathrm{Nu_x} = \frac{q_w}{(T_w - T_\infty)},$$

$$\mathrm{Nu_x} = \frac{-x(T_w - T_\infty)\theta'(0)\sqrt{\frac{U}{vx}}}{(T_w - T_\infty)}$$

$$\mathrm{Nu_x} = -\theta'(0)\sqrt{\frac{Ux}{v}} \tag{4.66}$$

Substituting $\sqrt{Re_x}$ into the $\mathrm{Nu_x}$ expression

$$\mathrm{Nu_x} = -\theta'(0)\sqrt{Re_x}$$

$$\frac{\mathrm{Nu_x}}{\sqrt{Re_x}} = -\theta'(0) \tag{4.67}$$

4.3 Conclusion

The transformation of partial differential equations into ordinary differential equations using similarity variables simplifies the problem while preserving accuracy. This approach is crucial for analysing boundary layer heat transfer and fluid flow efficiently.

CHAPTER 5
RESULT AND DISCUSSION

5.1 Introduction

This chapter presents the findings of the numerical analysis of the effect of velocity slip on unsteady magnetohydrodynamic (MHD) Maxwell fluid flow caused by a stretching sheet. The results are explained to determine the effects of key parameters such as velocity slip, magnetic field strength, thermal radiation, porosity, and heat generation/absorption on fluid velocity and temperature profiles. The findings are shown in plots and tables to assist in the visualization of the changes in boundary layer, skin friction coefficient, and heat transfer rate.

5.2 Result and Discussion

The governing partial differential equations were transformed into ordinary differential equations using similarity transformations and solved numerically using the Runge-Kutta-Fehlberg (RKF45) method in MAPLE software. The results were validated against existing literature to ensure accuracy. The effects of varying parameters on the fluid flow and heat transfer characteristics are discussed below.

Table 5.1 Comparison of skin friction coefficient $-f''(0)$ with previous study.

A	Sharidan et al. (2006)	Mukhopadhyay et al. (2013)	Sonam and Yadav (2024)	Present Result
0.8	1.261042	1.261479	1.26104261	1.2610426127

Table 5.1 validates the skin friction coefficient $f''(0)$ for unsteady MHD Maxwell fluid flow over stretching surface by comparing results with Sharidan et al. (2006), Mukhopadhyay et al. (2013), and Sonam and Yadav (2024) at $A = 0.8$ (unsteadiness parameter). The present study's numerical outcomes, obtained using RKF45 method by Maple Software, showed excellent agreement with these previous studies, confirming the accuracy of the numerical approach and transformed ordinary differential equations.

5.3 Result of Skin Friction Coefficient *f''(0)*, Heat transfer Rate *-θ'(0)*, Velocity Profile and Temperature Profile

5.3.1 Velocity slip parameter, λ

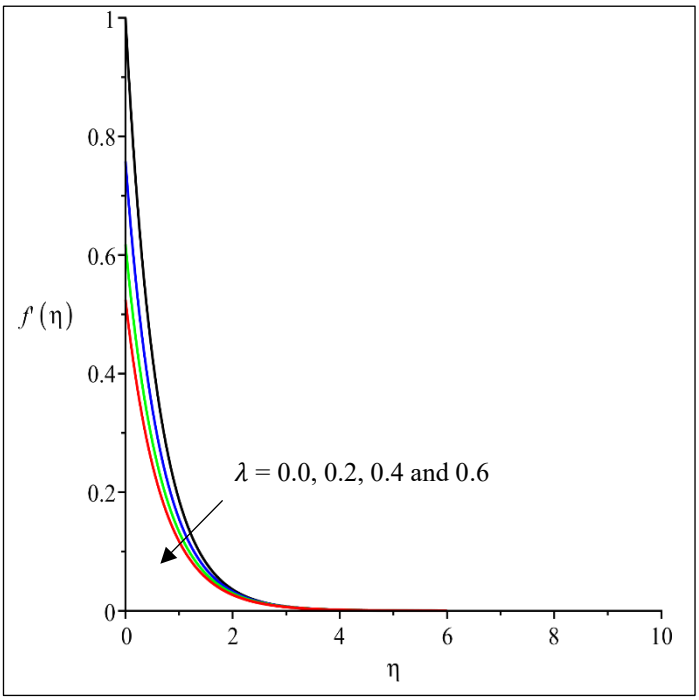

Figure 5.1 Velocity profile for multiple values of λ

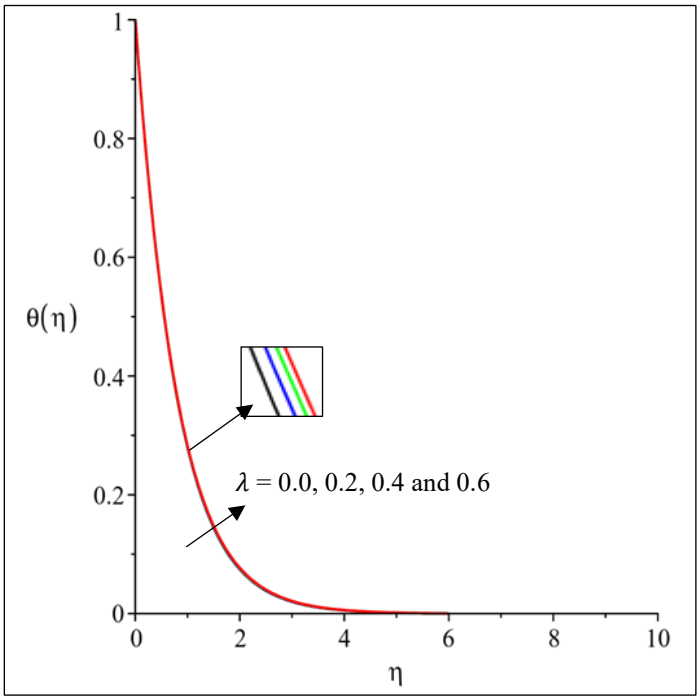

Figure 5.2 Temperature profile for multiple values of λ

Table 5.2 $-f''(0)$ and $-\theta'(0)$ when β=0.1, K_1=0.5, Pr=0.7, Ec=0.2, Q=-5.0, S=0.1, M=1.0 and A=0.1 for λ various values.

$\boldsymbol{\lambda}$	$\boldsymbol{-f''(0)}$	$\boldsymbol{-\theta'(0)}$
0.0	1.681899	1.148538
0.2	1.209732	1.162497
0.4	0.954830	1.167228
0.6	0.792314	1.169102

Figure 5.1 demonstrate the velocity profiles at various values of λ, whereas Figure 5.2 indicates temperature profiles for varying slip parameter, λ. Figure 5.1 shows a reduction in momentum boundary layer thickness with increasing λ. As a result, the gradient of the velocity profile decreases. Therefore, as presented in Table 5.2, the absolute value of the skin friction coefficient decreases accordingly. Figure 5.2 demonstrates a slight increase in the thermal boundary layer thickness as λ increases. This suggests a slight decrease in the temperature profile gradient. Hence, the heat transfer rate decreases with an increase in λ.

Velocity slip can be defined as state where the fluid just above the boundary layer is moving itself on the surface, instead of sticking on it fully. As λ is increased the fluid feels more ease in slipping along the surface hence minimizes drag force on the boundary layer. As a result, the drag coefficient of the skin ends up being smaller since there is reduction of the interaction between the fluid and the surface. At that, effective heat transfer gladly presupposes substantial contact of the fluid with the surface. And there is more of an increase in λ. The effect of λ minimizes this contact causing reduced rate of heat transfer between the surface and the fluid.

5.3.2 Various unsteadiness parameter, A

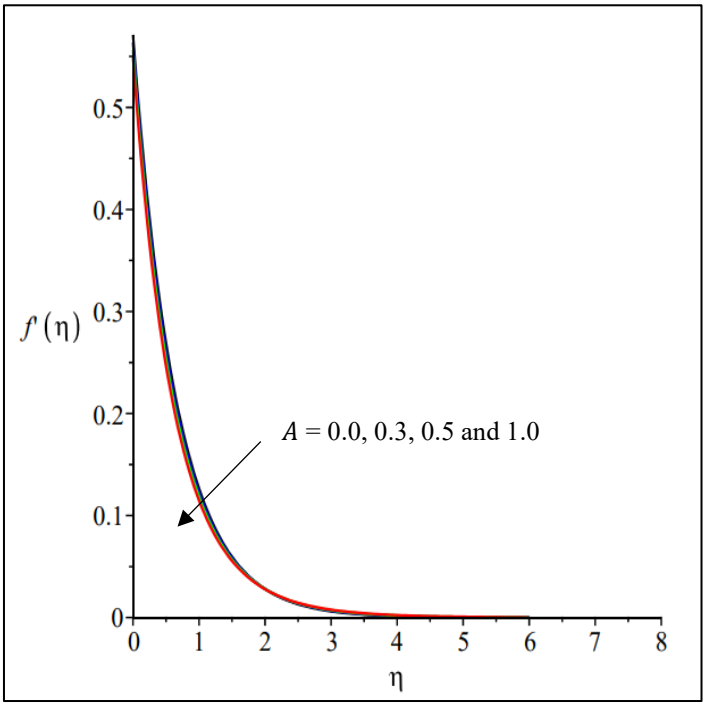

Figure 5.3 Velocity profile for multiple values of A

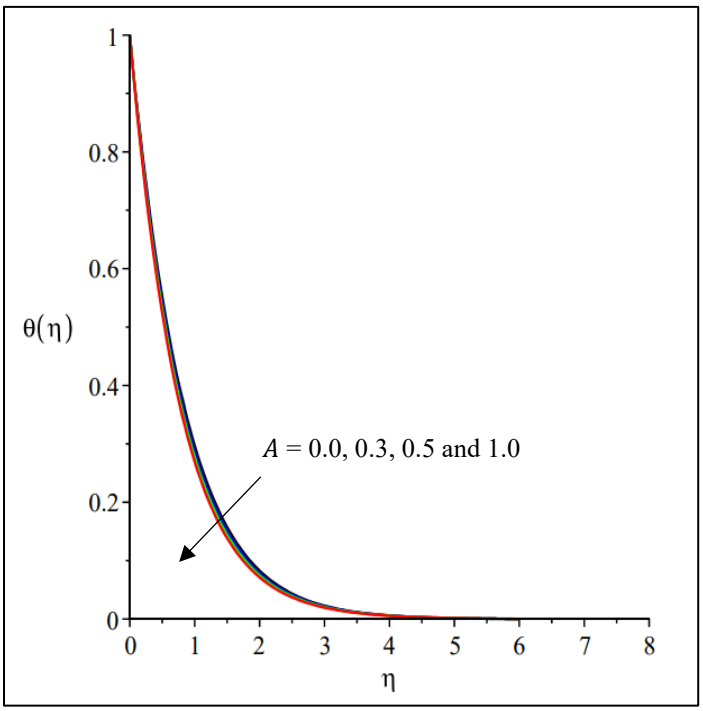

Figure 5.4 Temperature profile for multiple values of A

Table 5.3 $-f''(0)$ and $-\theta'(0)$ when β=0.1, K_1=0.5, Pr=0.7, Ec=0.2, Q=-5.0, S=0.1, M=1.0 and λ=0.5 for A various values.

$\boldsymbol{A}$	$\boldsymbol{-f''(0)}$	$\boldsymbol{-\theta'(0)}$
0.0	0.857961	1.147437
0.3	0.873079	1.188980
0.5	0.887554	1.248974
1.0	0.901412	1.343580

Figure 5.3 demonstrate the velocity profiles and temperature profile for various unsteadiness parameter, A respectively. Figure 5.3 shows the momentum boundary layer thickness decrease as A increases. As a result, the velocity profile gradient increases. Therefore, the absolute value of skin friction coefficient increases as shown in Table 5.3. Figure 5.4 shows the decreases of thermal boundary layer thickness. This leads to the temperature profile gradient on the surface to increases. Therefore, the heat transfer rate increases as A increases.

When the unsteadiness parameter A increases, the surface stretches more quickly over time. This faster stretching pulls the fluid along the surface more strongly, which makes the momentum boundary layer thinner. As a result, the fluid near the surface moves faster, increasing the velocity gradient and the skin friction coefficient, as shown in Table 5.3. At the same time, the thermal boundary layer also becomes thinner. This means heat stays closer to the surface, causing the temperature gradient to become steeper. With a steeper gradient, more heat is transferred from the surface to the fluid. Therefore, as A increases, the heat transfer rate also increases.

5.3.3 Various porosity parameter, K_1

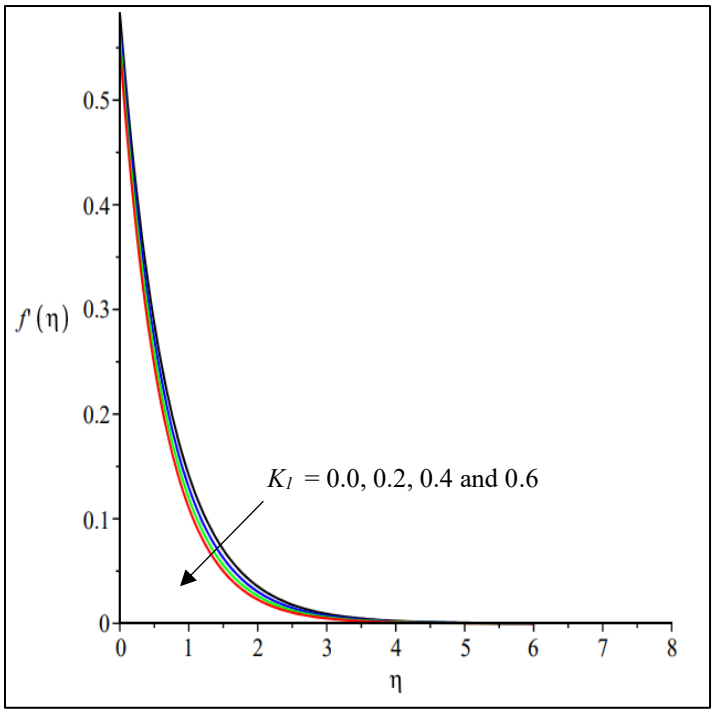

Figure 5.5 Velocity profile for multiple values of K_1

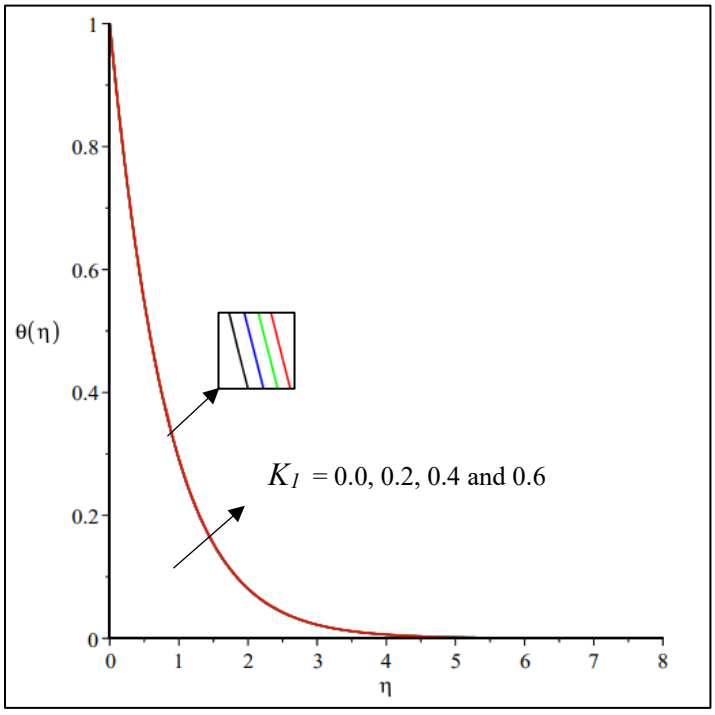

Figure 5.6 Temperature profile for multiple values of K_1

Table 5.4 $-f''(0)$ and $-\theta'(0)$ when β=0.1, A=0.1, Pr=0.7, Ec=0.2, Q=-5.0, S=0.1, M=1.0 and λ=0.5 *for* K_1 various values.

K_1	$-f''(0)$	$-\theta'(0)$
0.0	0.832672	1.169355
0.2	0.855059	1.168685
0.4	0.875752	1.168072
0.6	0.894979	1.167509

Figures 5.5 and 5.6 indicates the velocity and temperature profiles for various porosity parameter, K_1 respectively. Figure 5.5 shows the momentum boundary layer thickness decreases as K_1 increases. This result in an increase in the gradient of the velocity profile. As a result, there is an increase in the absolute value of the skin friction coefficient such in Table 5.4. Figure 5.6 shows a slight increase in thermal boundary layer thickness as K_1 increases. As a result, the temperature gradient at the surface slightly decreases, which result in a lower heat transfer rate.

When the porosity parameter K_1 increases, it means the fluid is passing through a more porous material. This added resistance makes it harder for the fluid to flow freely, pushing it closer to the surface. As a result, the velocity near the surface increases, making the momentum boundary layer thinner and the velocity gradient steeper. This explains the rise in the skin friction coefficient, as shown in Table 5.4. At the same time, the porous structure slightly affects how heat spreads through the fluid. The thermal boundary layer becomes a bit thicker, which reduces the temperature gradient at the surface. Because of this, the heat transfer rate becomes slightly lower.

5.3.4 Various magnetic parameter, M

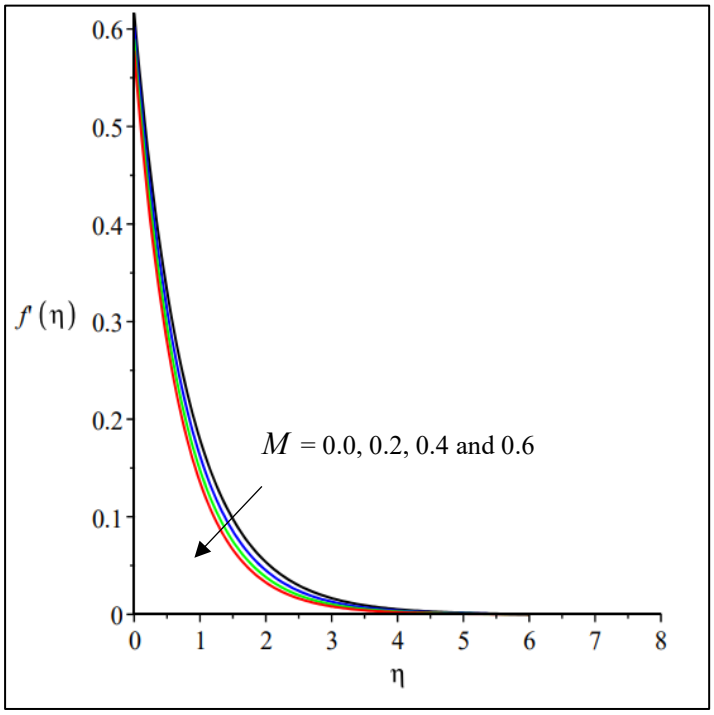

Figure 5.7 Velocity profile for multiple values of M

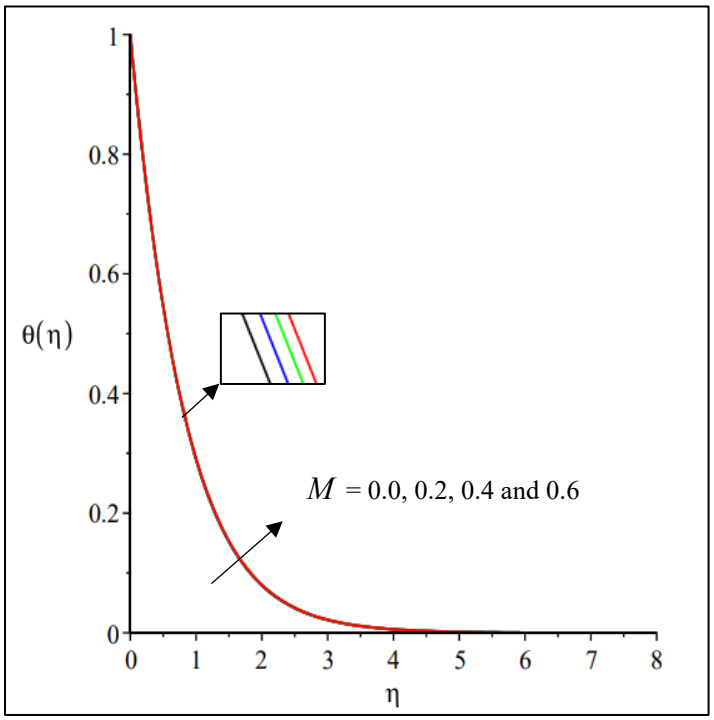

Figure 5.8 Temperature profile for multiple values of M

Table 5.5 $-f''(0)$ and $-\theta'(0)$ when β=0.1, A=0.1, Pr=0.7, Ec=0.2, Q=-5.0, S=0.1, K_1=0.5 and λ=0.5 for M various values.

$\boldsymbol{M}$	$\boldsymbol{-f''(0)}$	$\boldsymbol{-\theta'(0)}$
0.0	0.767239	1.176146
0.2	0.795277	1.173796
0.4	0.820758	1.171754
0.6	0.844093	1.169961

Figures 5.7 and 5.8 illustrate the velocity and temperature profile for various magnetic parameter, M. Figure 5.7 illustrates the momentum boundary layer thickness decreases as M increases. As a result, the gradient of the velocity profile decreased. Therefore, the absolute value of the skin friction coefficient decreases, as shown in Table 5.5. An increase in M results in a slight thickening of the thermal boundary layer, as shown in Figure 5.8. This indicates that the gradient of the temperature profile becomes slightly decreases. Thus, the heat transfer rate decreases as the magnetic parameter M increases.

As the magnetic parameter M increases, this opposing force gets stronger, making it harder for the fluid to move near the surface. This causes the fluid to slow down, which reduces the velocity and weakens the friction between the fluid and the surface explaining why the skin friction coefficient becomes smaller. Since moving fluid helps carry heat away from the surface, the slower motion also means less heat is transferred. In simple terms, a stronger magnetic field slows down the flow and reduces its ability to transport heat, leading to lower heat transfer efficiency.

5.3.5 Various Prandtl number, *Pr*

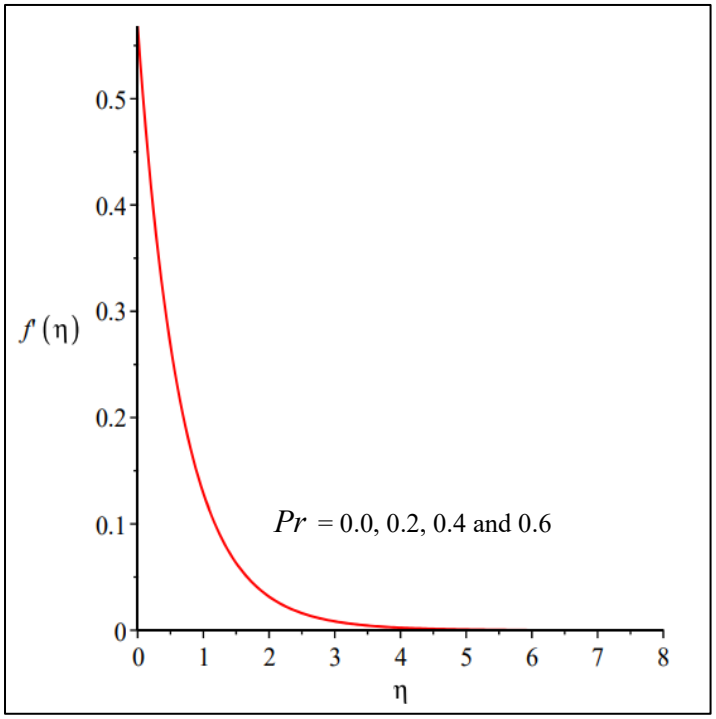

Figure 5.9 Velocity profile for multiple values of *Pr*

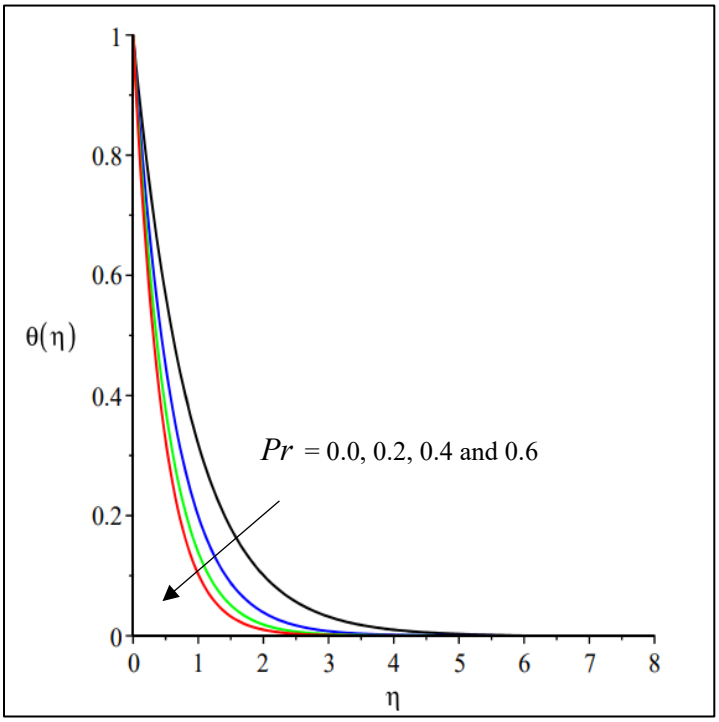

Figure 5.10 Temperature profile for multiple values of *Pr*

Table 5.6 $-f''(0)$ and $-\theta'(0)$ when β=0.1, A=0.1, M=1.0, Ec=0.2, Q=-5.0, S=0.1, K_1=0.5 and λ=0.5 *for Pr* various values.

Pr	$-f''(0)$	$-\theta'(0)$
0.0	0.863322	1.127207
0.2	0.863322	1.577138
0.4	0.863322	1.915647
0.6	0.863322	2.196536

Figures 5.9 and 5.10 present the velocity and temperature profiles for different Prandtl numbers, *Pr*. The figure 5.9 indicates that the momentum boundary layer was not influenced by the rise of *Pr*. As a result, the velocity profile gradient is not affected by this resultant effect. This is further confirmed by Table 5.6, where the skin friction coefficient remains constant regardless of *Pr*. Figure 5.10 shows that the thermal boundary layer thickness decreases with increasing Prandtl number, *Pr*. This results in an increase in the temperature profile gradient. Therefore, the surface heat transfer rate increases with higher Prandtl number, *Pr*.

An increase in Prandtl number is equivalent to an increase of fluid viscosity thereby increasing rate of heat transfer between the surface and the fluid. A larger Prandtl number indicates that the fluid will have decreased thermal diffusivity as compared to momentum diffusivity. That means that heat conduction is not so dominant in respect to the convection. The more powerful convection systems are in the process of convective heat transfer, the higher the convection level is about the transfer of the thermal energy resulting in the more effective general heat transfer represented as the transfer of the thermal energy out of the surface into the fluid.

5.4 Conclusion

In conclusion, the results presented in this chapter demonstrate how parameters like velocity slip, unsteadiness, porosity, magnetic field, and thermal effects influence the flow and heat transfer of Maxwell fluid. The findings are consistent with the numerical trends reported by Sonam and Yadav (2024) and agree with earlier observations by Sharidan et al. (2006) and Mukhopadhyay et al. (2013). This consistency supports the accuracy of the current model and its relevance in practical thermal-fluid systems.

CHAPTER 6
CONCLUSION AND RECOMMENDATION

6.1 Introduction

This chapter will present the conclusions of the study on the effects of velocity slip in unsteady Maxwell fluid flow over a stretching surface.

6.2 Conclusion

From this study, it is shown that the results obtained are in good agreement with results obtained by Sonam and Yadav (2024), Sharidan et al. (2006) and Mukhopadhyay et al. (2013). The presence of velocity slip parameter, porosity parameter, magnetic parameter, Prandtl number and unsteadiness parameter were considered in this study.

It was found that, the skin friction was minimized, and the thickness of thermal boundary layer was marginally thinner when the velocity slip parameter was amplified because of the reduced intensity of fluid-wall interaction. The porosity parameter added to the resistance of flow, which added skin friction and decreased thermal transfer.

Same way, a higher magnetic field increased the resistance of flow but it reduced heat transport because of Lorentz force. Increased Prandtl number resulted in a thin thermal boundary layer, which increased the heat transfer performance. Finally, the instability of the whole system led to enhanced mixing of the fluid and shear stresses close to the surface, which added positively to heat transfer. Altogether, it is an important study based on the understanding of the importance of these parameters in determining or influencing behaviour of Maxwell fluids in real thermal-fluid systems.

6.3 Recommendation

The results may be directly used to optimize the processes of polymer manufacture, thermal regulating systems, and electromagnetic stream direction. In designing a high-efficiency heat exchanger or coating system, engineers ought to consider incorporation of velocity slip parameters as well as porosity parameters. The next way forward is to investigate temperature-dependent fluid characteristics, viscoelastic models of fluids and interaction of different physical effects to improve the accuracy of predictions. These advances will also shed more light on complicated boundary layer behaviours in engineering practice.

REFERENCES

Cajot, F., Doussan, C., Hartmann, S., & Beltrame, P. (2025). Model of drop infiltration into a thin amphiphilic porous medium. *Journal of Colloid and Interface Science*.

Geraeilinezhad, M., Afrouzi, H. H., Jahanian, O., & Mehrizi, A. A. (2023). Numerical investigation of pseudoplastic fluid flow and heat transfer in a microchannel under velocity slip effect. *Engineering Analysis with Boundary Elements*, *155*, 501-510. https://doi.org/10.1016/j.enganabound.2023.06.021

Hassan, W. U., Shabbir, K., Zeeshan, A., & Ellahi, R. (2025). Regression analysis for thermal transport of fractional-order magnetohydrodynamic Maxwell fluid flow under the influence of chemical reaction using integrated machine learning approach. *Chaos, Solitons & Fractals*, *191*. https://doi.org/10.1016/j.chaos.2024.115927

Iqbal, A., Abbas, T., Shahzad, A., Nawaz, R., & Ahmad, B. (2024). Analysis of unsteady flow of Cu− EG based nanoparticle of different shapes in the presence of joule heating over stretching surface. *Nano-Structures & Nano-Objects*, *39*, 101241.

Kamran, T., Afzal, F., & Riaz, M. B. (2025). Numerical simulation of graphene Maxwell nanofluid flow with thermal radiation and slips conditions along a linearly stretched sheet. *Results in Engineering*, *25*. https://doi.org/10.1016/j.rineng.2025.104487

Kezzar, M., Talbi, N., Rafik Sari, M., Nehal, A., Sharifpur, M., Kumar, R., Gharib, N., Salsoul, W., & Fatiha, H. (2023). Velocity-slip boundary conditions and shape factor effects on MHD hybrid nanofluid flow via converging/diverging channels. *Journal of Magnetism and Magnetic Materials*, *587*. https://doi.org/10.1016/j.jmmm.2023.171215

Krishna, M. V., & Kumar, A. V. (2024). Chemical reaction, slip effects and non-linear thermal radiation on unsteady MHD Jeffreys nanofluid flow over a stretching sheet. *Case Studies in Thermal Engineering*, *55*, 104129.

Maraj, E. N., Zehra, I., & SherAkbar, N. (2022). Rotatory flow of MHD (MoS2-SiO2)/H2O hybrid nanofluid in a vertical channel owing to velocity slip and thermal periodic conditions. *Colloids and Surfaces A: Physicochemical and Engineering Aspects*, *639*. https://doi.org/10.1016/j.colsurfa.2022.128383

Memon, M. A., Jacob, K., Lanjwani, H. B., & Mahmoud, E. E. (2024). Darcy-Forchheimer MHD micropolar water based hybrid nanofluid flow, heat and mass transfer features past on stretching/shrinking surface with slip and radiation effects. *Results in Engineering*, *23*, 102534.

Mukhopadhyay, S., Ranjan De, P., & Layek, G. (2013). Heat transfer characteristics for the Maxwell fluid flow past an unsteady stretching permeable surface embedded in a porous medium with thermal radiation. *Journal of Applied Mechanics and Technical Physics*, *54*, 385-396.

Olabode, J. O., Idowu, A. S., Akolade, M. T., & Titiloye, E. O. (2021). Unsteady flow analysis of Maxwell fluid with temperature dependent variable properties and quadratic thermo-solutal convection influence. *Partial Differential Equations in Applied Mathematics*, *4*. https://doi.org/10.1016/j.padiff.2021.100078

Reddy, N. N., & Goud, B. S. (2025). Slip effects on MHD heat and mass transfer flow through porous medium over an exponentially stretching sheet in existence of suction. *Journal of Radiation Research and Applied Sciences*, *18*(2). https://doi.org/10.1016/j.jrras.2025.101338

Salahuddin, T., Awais, M., & Muhammad, S. (2024). Featuring the aspects with temperature dependent viscosity of inclined MHD Williamson fluid along with heat source/sink, Soret and Dufour effects: A predictor-corrector approach. *International Communications in Heat and Mass Transfer*, *159*, 108178.

Sanderse, B., & Trias, F. (2025). Energy-consistent discretization of viscous dissipation with application to natural convection flow. *Computers & Fluids*, *286*, 106473.

Shah, F. A., Mikhaylov, A., & Haq, E. U. (2025). Numerical framework for investigating MHD heat and mass transfer in nanofluid flow over 2-D boundary layers in a porous medium: A variation of parameters method approach. *Results in Engineering*, *25*, 103547.

Shah, S., Rafiq, N., Abdullah, F. A., Atif, S. M., & Abbas, M. (2022). Slip and radiative effects on MHD Maxwell nanofluid with non-Fourier and non-Fick laws in a porous medium. *Case Studies in Thermal Engineering*, *30*. https://doi.org/10.1016/j.csite.2022.101779

Sharidan, S., Mahmood, M., & Pop, I. (2006). Similarity solutions for the unsteady boundary layer flow and heat transfer due to a stretching sheet. *Applied Mechanics and Engineering*, *11*(3), 647.

Sharma, B. K., & Gandhi, R. (2022). Combined effects of Joule heating and non-uniform heat source/sink on unsteady MHD mixed convective flow over a vertical stretching surface embedded in a Darcy-Forchheimer porous medium. *Propulsion and Power Research*, *11*(2), 276-292. https://doi.org/10.1016/j.jppr.2022.06.001

Sonam, & Yadav, R. S. (2024). Numerical study of MHD Maxwell fluid flow from a stretching surface with radiation impact. *Physics Letters A*, *526*. https://doi.org/10.1016/j.physleta.2024.129976

Vishwanatha, U. B., Reddy, Y. D., Barmavatu, P., & Goud, B. S. (2023). Insights into stretching ratio and velocity slip on MHD rotating flow of Maxwell nanofluid over a stretching sheet: Semi-analytical technique OHAM. *Journal of the Indian Chemical Society*, *100*(3). https://doi.org/10.1016/j.jics.2023.100937

APPENDICES

For λ vary

```
> λ varying :
> restart :
> with(plots) : β := 0.1 : K1 := 0.5 : Pr := 0.7 : N := 1 : Ec := 0.2 : Q := -5.0 : S := 0.1 : M :=
      1.0 : A := 0.1 :
> eq1 := A·(diff(f(η), η) + η/2·diff(f(η), η, η)) + diff(f(η), η)^2 − f(η)·diff(f(η), η,
      η) + β·(f(η)^2·diff(f(η), η, η, η) − 2·f(η)·diff(f(η), η)·diff(f(η), η, η))
      = diff(f(η), η, η, η) − K1·diff(f(η), η) − M·diff(f(η), η);
```

$$eq1 := 0.1\left(\frac{d}{d\eta}f(\eta)\right) + 0.05000000000\,\eta\left(\frac{d^2}{d\eta^2}f(\eta)\right) + \left(\frac{d}{d\eta}f(\eta)\right)^2 \tag{1}$$
$$-f(\eta)\left(\frac{d^2}{d\eta^2}f(\eta)\right) + 0.1\,f(\eta)^2\left(\frac{d^3}{d\eta^3}f(\eta)\right)$$
$$-0.2\,f(\eta)\left(\frac{d}{d\eta}f(\eta)\right)\left(\frac{d^2}{d\eta^2}f(\eta)\right) = \frac{d^3}{d\eta^3}f(\eta) - 1.5\left(\frac{d}{d\eta}f(\eta)\right)$$

```
> eq2 := A·(2·θ(η) + η/2·diff(θ(η), η)) = f(η)·diff(θ(η), η) − diff(θ(η), η)·θ(η)
      + 1/Pr·(1 + 4·N/3)·diff(θ(η), η, η) + Ec·(diff(f(η), η, η)^2 + M·diff(f(η), η)^2)
      + Q·θ(η);
```

$$eq2 := 0.2\,\theta(\eta) + 0.05000000000\,\eta\left(\frac{d}{d\eta}\theta(\eta)\right) = f(\eta)\left(\frac{d}{d\eta}\theta(\eta)\right) \tag{2}$$
$$-\left(\frac{d}{d\eta}\theta(\eta)\right)\theta(\eta) + 3.333333333\left(\frac{d^2}{d\eta^2}\theta(\eta)\right) + 0.2\left(\frac{d^2}{d\eta^2}f(\eta)\right)^2$$
$$+0.20\left(\frac{d}{d\eta}f(\eta)\right)^2 - 5.0\,\theta(\eta)$$

```
> bcs1 := f(0) = S, D(f)(0) = 1 + λ·D(D(f))(0), θ(0) = 1;
```

$$bcs1 := f(0) = 0.1,\ D(f)(0) = 1 + 0.5\,D^{(2)}(f)(0),\ \theta(0) = 1 \tag{3}$$

```
> bcs2 := D(f)(6) = 0, θ(6) = 0;
```

$$bcs2 := D(f)(6) = 0,\ \theta(6) = 0 \tag{4}$$

```
> L := [0.0, 0.2, 0.4, 0.6, 0.8] :
> for k from 1 to 4 do K := dsolve(eval({eq1, eq2, bcs1, bcs2}, λ = L[k]), [f(η), θ(η)],
      numeric, output = listprocedure); X||k := rhs(K[3]); XP||k := rhs(K[4]); Y||k :=
      rhs(K[5]); YP||k := -rhs(K[6]) end do:
> p1 := plot([X||(1)], 0..10, labels = [η, f'(η)], thickness = 1, color = black):
> p2 := plot([X||(2)], 0..10, labels = [η, f'(η)], thickness = 1, color = blue):
> p3 := plot([X||(3)], 0..10, labels = [η, f'(η)], thickness = 1, color = green):
> p4 := plot([X||(4)], 0..10, labels = [η, f'(η)], thickness = 1, color = red):
> display(p1, p2, p3, p4);
```

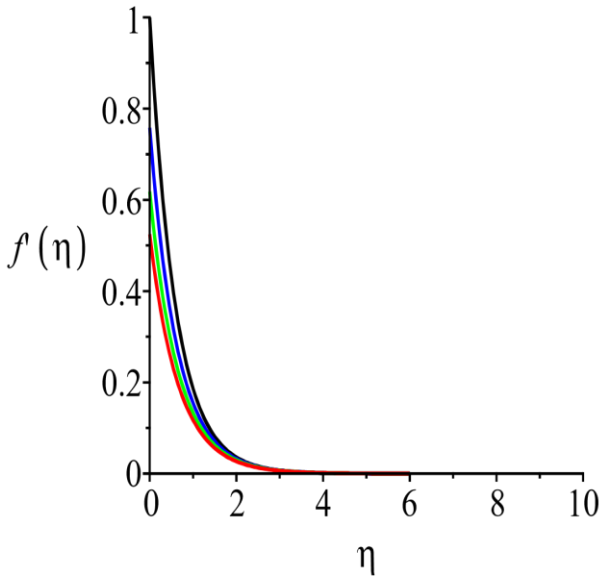


```
> a1 := plot([Y||(1)], 0..10, labels = [η, θ(η)], thickness = 1, color = black):
> a2 := plot([Y||(2)], 0..10, labels = [η, θ(η)], thickness = 1, color = blue):
> a3 := plot([Y||(3)], 0..10, labels = [η, θ(η)], thickness = 1, color = green):
> a4 := plot([Y||(4)], 0..10, labels = [η, θ(η)], thickness = 1, color = red):
> plots:-display(a1, a2, a3, a4);
```

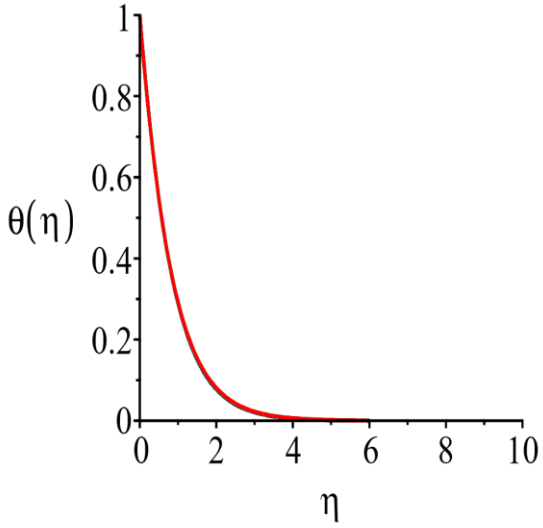


```
> print([XP||(1..4)(0)])
```

[−1.68189971252123, −1.20973206183803, −0.954830031223955, −0.792314444703305] **(5)**

```
> print([YP||(1..4)(0)])
```

[1.14853850367824, 1.16249739263830, 1.16722834629114, 1.16910258160570] **(6)**